NASA Contractor Report 165682

DEVELOPMENT OF LEAD SALT SEMICONDUCTOR LASERS FOR THE 9-17 MICRON SPECTRAL REGION

K. J. Linden, J. F. Butler
K. W. Nill, R. E. Reeder

LASER ANALYTICS, INC.
Bedford, MA 01730

CONTRACT NAS1-15190
MARCH 1981

National Aeronautics and
Space Administration

Langley Research Center
Hampton, Virginia 23665

TABLE OF CONTENTS

LIST OF FIGURES

fabricated from $Pb_{.966}Sn_{.034}Se$ and lasers 8292-10 and 8303-22 were fabricated from $Pb_{.927}Sn_{.073}Se$ corresponding to the 11.5 and 17.2 μm spectral regions, respectively.

2.13 Comparison of emission spectra from laser 8292-2 taken on October 20, 1978 and again on November 13, 1979. In both cases, I = 2000 mA, CW. Differences in power reading could, in part, be due to different power meters. The shift of 6 cm^{-1} towards higher wavenumbers is possibly due to a slight thermal resistance increase.

2.14 Top: Schematic diagram of a cross-section of wafer D1785S showing electrical contact stripe configuration. Bottom: Electron beam micrograph of this same wafer taken at 1240X magnification showing one contact stripe opening in the insulating layer. Stripe width is 12 μm.

2.15 Emission spectra of lasers from wafer D1785 ($Pb_{0.955}Sn_{0.045}Se$) at 2000 mA and 15 K. The 3 lasers on the left side are not striped (NS) while the 3 lasers on the right side are contact striped (SS = shallow etch of 1 μm and SD = deep etch of 3 μm prior to metallization).

2.16 Drawing of photomasks used for obtaining diffused stripe lasers with various stripe widths.

2.17 Photomicrographs of two sections of the same crystal, the left one as grown and the right one previously coated with the diffusion masking materials. Both surfaces have been subjected to an EPD measurement. Most of the entire surface of the right one shows a high EPD, indicative of crystal surface dislocations. Magnified 40X.

2.18 Emission spectra of lasers 0025-26 (top curve, non-striped laser) and 0023-18 (bottom curve, striped laser) at 2000 mA.

2.19 Optical characteristics of laser 9093-21, comprising one of the 2 lasers kept at Laser Analytics for 11 months prior to delivery to LASL. During this period, the laser was periodically checked for stability.

2.20 Optical characteristics of laser 9110-3, comprising one of the 2 lasers kept at Laser Analytics for 11 months prior to delivery to LASL. During this period, the laser was periodically checked for stability.

LIST OF TABLES

1.0 INTRODUCTION

1.1 Need for the Program

High performance PbSnSe tunable diode lasers are of considerable interest to the NASA/Langley Research Center for use as local oscillators in the Laser Heterodyne Spectrometer (LHS) program and to the Los Alamos Scientific Laboratories for spectroscopy in support of Laser Isotope Separation (LIS) programs. These lasers possess many unique and highly desirable features for such applications, including wide wavelength tunability, narrow linewidth and very small size. However, they have only been marginally able to meet the unusually stringent requirements of LHS and LIS in regard to properties such as output power, reliability and run-to-run reproducibility. This report describes the methodology and results of a research and development program directed toward improving the performance of PbSnSe lasers in these areas. The three major objectives of the program were as follows.

a. Demonstrate laser output powers of 500 μW per mode in the 9-12 μm bands at operating temperatures greater than 30 K in two spectral regions, and in excess of 200 μW per mode in the 16-17 μm region at operating temperatures greater than 18 K.

b. Increase the reliability and yield by performing a series of diagnostic measurements on the devices to identify and characterize failure mechanisims; the goal is a shelf storage life of one year.

c. Improve the tuning stability with goals of:

   1. a frequency reproducibility of better than 0.1 cm^{-1} after a temperature cycling from 18 K to 300 K and back to 18 K and,

   2. a tuning rate reproducibility of better than 20% after a temperature cycle of 18 K to 300 K and back to 18 K.

The objectives, specific program goals and specifications were met in the following areas:

a. All ten of the NASA lasers (9-12 μm band) had CW output powers in excess of 100 μW per mode at 15 K.

b. Two of the NASA lasers had single mode output powers in excess of 1 mW (one had 2.7 mW).

c. NASA measurements verified that five of the NASA lasers emitted in excess of 500 μW/mode and that one of the lasers met all program goals and objectives (i.e., > 500 μW/mode at > 30 K within the specified wavelength region).

d. All of the NASA lasers operated within one of the two specified wavelengths in the 9.2 and 11.2 μm spectral regions.

e. All lasers delivered to LASL met the program objectives of output power > 200 μW/mode at T > 18 K.

Test results on the 10 lasers delivered to NASA are summarized in attachment A. In addition, a number of significant new observations were made which have increased our understanding of the complex technology of Pb-Salt diode lasers, and a somewhat clearer picture of the fundamental causes of long-term degradation has emerged. Major results are summarized in Section 1.3 below.

1.2 Background

1.2.1 The CID Technology

All of the lasers for this program were fabricated using the CID technology, described in a previous publication. (1) CID lasers

are single heterojunction (SH) devices, with the heterojunction situated within a few micrometers from the surface and the p-n junction lying somewhat deeper. Excited carriers are injected from the p-n junction toward the heterojunction and confined within the narrow region between the junctions. In addition to carrier confinement, this structure provides partial optical confinement as a result of the relatively large dielectric discontinuity at the heterojunction and smaller discontinuity at the pn-junction.

The technology of Pb-salt lasers is based to a large degree on controlling the wide deviations from stoichiometry and their effects on charge carrier type and concentration (2). The feasibility of the CID structure, in particular, depends on the diffusion and interdiffusion parameters having values such that a region of wider bandgap at the surface can be diffused simultaneously with the diffusion of a deeper p-n junction. Use of an n-skin, p-bulk structure ensures that injection of carriers occurs from the bulk p-region, toward the heterojunction, because the equilibrium carrier concentrations in p-type PbSnSe is much higher than in n-type material under the conditions of the diffusion process. As discussed below, one aspect of the program was concerned with attempting to optimize the distance between the pn-junction and the heterojunction.

1.2.2 Considerations Related to Power Output

Tunable diode lasers operating in the 9-17 μm region, emit typical power outputs of less than 300 microwatts overall and less than 50 microwatts in a single mode. This corresponds to an external quantum efficiency of 0.2% - 0.4% (two-ended). Considerably higher power outputs have been observed from exceptional devices fabricated in our laboratory, 5 milliwatts at 15 μm, for example, corresponding to an external quantum efficiency of 6%. There is no known theoretical bar to achieving external quantun efficiencies near 50% and corresponding 15 μm power outputs of 42 milliwatts.

Thus, the program objectives for output power outlined above were believed to be achievable, although at the limits of feasibility of the existing technology. It was anticipated that one result of the program would be an improved understanding of the technology which would lead to attainment of higher output powers on a more routine basis.

1.2.3 Long Term Reliability

PbSnSe diode lasers have in the past been plagued by two failure mechanisms of particular significance: temperature cycling failure and room temperature contact degradations.

Temperature cycling failure is thought to be primarily related to the integrity of the laser package, i.e., the structure consisting of heat sink, crystal mounting platform, electrical contact wires, insulators, etc. The package must withstand repeated cyclings over wide temperature differences between about 10 K and room temperature, a range within which materials properties such as thermal expansion coefficients, and thermal conductivity change strongly and are not well characterized. Package design had recently received considerable attention by Laser Analytics, Inc., and was believed not to pose a significant problem. Cycling tests carried out as part of the program subsequently verified that temperature cycling failures did not often occur with PbSnSe lasers manufactured by Laser Analytics. Room temperature contact degradation was, however, a significant problem. The general phenomena observed were the following.

a. The series resistance, as determined from the slope of the linear portion of the forward current-voltage characteristics, increased with time.

b. The thermal impedance of the contact between the laser crystal and the heat sink increased with time. This was evidenced by an increased current tuning rate which, in some cases, occurred without any change in series resistance.

c. Not every laser degraded. At the beginning of the program, it is believed that more than 50% of initially acceptable lasers exhibited severe degradation within a period of six months.

The increases in series resistance and thermal impedance caused a gradual increase in tuning rate, eventually to an unacceptably high level. In a severely degraded device, application of bias current caused complete burn-out as a result of runaway I^2R heating at the contacts. The time for complete failure varied from less than a month for the worst devices to over a year in other cases.

The causes of contact degradation were not clearly understood at the beginning of the program, and previous considerations of this problem had been complicated by the existence of simultaneous package failure, surface leakage currents unrelated to contact degradation, and other phenomena. It was, in fact, a significant task to sort out the various observations and isolate and define specific, solvable problems.

It has long been known that Au layers could be made to produce low-resistance, non-rectifying contact to p-type Pb-salt semiconductors, whereas In on p-type surfaces usually produces rectifying, unusable contacts. (3) This is easily explained in terms of standard Schottky barrier theory and suggests that interface surface states do not play a strong role in these contacts. (4) The fact that Au and In interact and form alloys at room temperature has long been a well known source of problems in the semiconductor industry. The interaction between Au and In films was recently studied by X-ray diffraction techniques and found to involve the formation of intermetallics such as Au-In, $AuIn_2$, Au_4In and Au_7In_3. (5) A very recent publication (6) has shown that the formation of these intermetallics can disrupt Au and In layers by forming voids and clumps, and thereby cause an increase in thermal impedance of GaAs diode lasers (possible effects on series resistance were not discussed). Earlier considerations about increasing contact resistance on Pb-salt lasers

centered on the concept that interaction with In lowered the work function of the Au layer, causing it to become rectifying for p-type Pb-salt surfaces. It was also recently suggested that the In diffuses into the p-surface and, being a donor, lowers the carrier concentration sufficiently to cause an increased resistivity. (7) The possibility of degradation on the n-type surface has apparently not been previously considered because pure In, without the presence of Au, has usually been used on this surface.

It has long been recognized that a barrier layer of metal such as Pt between the Au and In layers could prevent the Au-In interaction and Au-Pt-In contacts have been used on the p-surface of Pb-salt lasers. (8) However, a systematic study has never been conducted to demonstrate that reliable, long-life lasers resulted from these attempts.

1.2.4 Stripe Geometry Laser Studies

The electromagnetic cavity of a diode laser can be described in terms of a dielectric slab model, in which the active region has a refractive index, n_1, which is higher than that of the surrounding material, n_2. The geometry of the cavity is defined by the distance between its end faces, L, junction plane width, d_1 and transverse dimensions, d_2, (transverse to the junction plane). The distance d_2 may be precisely defined in a double heterostructure laser, but in a homojunction or CID (1) device, it is a complex quantity involving carrier densities in the n- and p-regions, carrier mobilities, cavity gain and other factors. The resonances of the cavity can be expressed in terms of longitudinal modes separated in frequency by $\Delta\nu = 1/2\ n_1 L(1 + \nu/n_1)\ (dn_1/d\nu))$ and transverse TE and TM modes of various orders. Each longitudinal mode will in general have several transverse components, the number being limited by the dimensions d_1 and d_2. The lowest order, TE_0 mode may occur for all dimensions of the cavity whereas higher order, TE and TM modes may exist only if d_1 or d_2 is large enough.

Different transverse modes for a given longitudinal mode may have slightly different frequencies as a result of geometrical dispersion, leading to satellite lines and consequent poor tuning characteristics.

Furthermore, high order modes emit in a multi-lobed spatial pattern which is highly undesirable for heterodyne applications since the combining of out-of-phase lobes at the mixer produces signal-degrading interferences. In view of these considerations it is important for NASA and LASL applications to attempt to restrict operation to the TE_0 mode. Analysis shows that higher order modes will be cut off if d_1 and d_2 are less than the quantity D defined by (9):

$$D = \lambda_0/(n_1^2 - n_2^2)^{1/2} \tag{1}$$

In a homojunction or CID laser, n_1 and n_2 differ by a small amount, perhaps less than 0.1%; in this case, the relevant dimension may be comparatively large. (In a double heterostructure laser the refractive index difference will be much larger, possibly by as much as 10%, and the dimension must be correspondingly smaller.) In the present program, an attempt was made to establish the maximum stripe width for TE_0 - only operation, i.e., to experimentally determine D in Equation (1) for lasers in the 9-17 μm region.

Stripe geometries were formed in this program by a diffusion masking technique. The use of other methods such as mesa-etching or buried junction would require additional extensive developmental efforts. As discussed below, sufficiently narrow junctions are not feasible using contact striping (i.e., the current confined by a simple stripe geometry electrical contact). The effective stripe width for a simple contact stripe on a homojunction or CID laser can be approximated by (10)

$$d_1 = d_{10} + \Delta S_1 \tag{2}$$

where
$$\Delta S_1 = 2\left(\frac{2kT}{er_S J_{th}(\infty)}\right)^{1/2} \tag{3a}$$

where r_s is the sheet resistance of the n- or p-skin and $J_{th}(\infty)$ is the threshold current density for a fully laterally confined structure. Equation (3a) may be expressed as:

$$\Delta S_1 = 2\left(\frac{2n\ \mu t\ k\ T}{J_{th}}\right)^{1/2} \tag{3b}$$

where n is the electron concentrations for an n-skin (replace by the hole concentration p for a p-skin), μ is the mobility of carriers in the skin and t is the skin thickness. Assume that at an operating temperature of 20 K, $n = 3 \times 10^{18}$ cm^{-3} (11), $\mu = 10^5$ cm^2/V s (12) and taking 500 amps/cm^2 as a representative value for $J_{th}(\infty)$, this becomes:

$$\Delta S_1 = 110 \sqrt{t} \qquad (3c)$$

where t and ΔS_1 are expressed in micrometers. With typical junction depths of 1-to-10 μm, it is apparent that the incremental component in Equation (2) is substantially larger than the 50 μm electrical contact stripe width used for production lasers. Decreasing t was not felt to be feasible since past experience has shown that very thin junctions do not perform well, possibly as a result of a superficial damaged region. Consequently, since the thrust of the experiment is toward narrower stripes, it is apparent that the contact stripe method would likely not be fruitful.

1.2.5 Diffusion Studies

In the single heterojunction, CID lasers utilized in this program, carriers are injected from the heavily doped base region into the n-skin, and reflected from a heterojunction near the surface. The distance from the heterojunction to the deeper-lying p-n junction thus defines the maximum active region width. Threshold currents are expected to decrease as the active region width decreases due to increased recombination efficiency and enhanced gain. However, as this width becomes too small, factors such as flattening of the junction at low current densities and other factors come into play and act to increase threshold current. In principle, then, one can design an optimum depth which will result in the lowest threshold current.

The goal at this portion of the program was to work out the diffusion parameters for precise control of junction depths in PbSnSe lasers. This capability should then make it possible to experimentally determine optimum junction depths, leading to improved device performance and, from comparing results with theory, a deeper understanding of the physics of these devices.

1.3 Major Results

The major results of the program are summarized in the following paragraphs.

(a) All ten of the NASA lasers (9-12 μm band) had measured CW output powers in excess of 100 μW per mode at 15K.

(b) Two of the NASA lasers had single mode output powers in excess of 1 mW (one had 2.7 mW).

(c) NASA measurements verified that five of the NASA lasers emitted in excess of 500 μW/mode and that one of the lasers met all program goals and objectives (i.e., >500 μW/mode at T>30K within the specified wavelength region).

(d) All of the NASA lasers operated within one of the two specified wavelengths in the 9.2 and 11.2 μm spectral regions.

(e) All lasers delivered to LASL met the program objectives of output power >200 μW/mode at T>18K.

(f) All lasers delivered under this contract met or exceeded contractual specifications with respect to operating temperatures. Seven of the ten lasers delivered to NASA and all six lasers to LASL operated at temperatures in excess of 30 K. The highest operating temperature for a delivered laser was 65 K.

(g) Two LASL lasers retained at LAI for one year for shelf life studies exhibited no significant change in electrical contact resistance after more than 10,000 hours of storage at room temperature.

(h) Lasers mounted in Laser Analytics' standard package showed no observable change in measured operating characteristics after 500 cycles between room temperature and 4.2 K.

(i) From a study of operating characteristics as a function of stripe width, it was tentatively concluded that the optimum stripe width of homostructure diffused devices is between approximately 12 and 25 μm for lasers in the 9-17 μm band.

(j) Lasers fabricated by a p into n type diffusion exhibited poorer performance than n into p devices, as expected from considerations related to the CID structure.

(k) Junction depths for n-into-p diffusions in PbSnSe were found to vary widely, with all parameters under careful control. The cause of this variation has not been determined and this problem is considered critical because of the importance of junction depth in the CID structure.

(l) From specific materials charcterization experiments and general observations during the course of the program, the following conclusions regarding contact degradation were drawn:

- Contacts of In to n-type PbSnSe can degrade at least as severely as Au-In contacts to p-type material. This is an important result since it throws serious doubt on published hypotheses attempting to explain the degradation solely in terms of a rectifying barrier formed on p-type material or diffusion of In into p-type material.
- Contact degradation is probably not due to variation of carrier concentration with time in the laser crystal.
- Observed changes in threshold current with time are due almost entirely to leakage currents (probably on exposed crystal surfaces) and are unrelated to contact degradation (the observed effect is generally an equal decrease in leakage and threshold currents with time).
- Auger Electron Spectroscopy measurements (i) show the presence of In on degraded p-type surfaces, indicating that In plays a role in degradation, (ii) do not provide evidence of diffusion of In into the crystal, and (iii) show that trace amounts of chemicals used in etching and cleaning crystal surfaces may be difficult to completely eliminate.
- The most likely cause of commonly observed contact degradation on PbSnSe lasers appears to be solid state migration involving the In bonding layer, with the consequent formation of intermetallic compounds and other structural changes in the layer, and loss of adhesion of the layer to the

crystal. An important new observation was that these hypothesized structural changes involve not only Au, but one or more components of the laser crystal.

- Contract degradation can be prevented by applying a barrier layer of platinum between the In layer the Au contact metallization layer.

2.0 THE EXPERIMENTAL PROGRAM

The general background and rationale for the experimental approaches were discussed in Section 1.2, above. Additional background information is presented for each specific subject of study below. The effort fell into the following broad areas.

A. Materials preparation and investigations (including diffusion studies and laser fabrication techniques).
B. Degradation studies.
C. Stripe geometry optimization.
D. Assembly and characterization of deliverable devices.

2.1 Materials Preparation and Investigation

2.1.1 Crystal Growth

A number of PbSnSe crystals were grown during the course of and for use in the program. Based upon the laser frequency requirements of both NASA-LRC and LASL, the following compositions were used.

Spectral Region cm^{-1}	Required x-value in $Pb_{1-x}Sn_xSe$ Crystals
893 - 943 (NASA)	0.033 - 0.035
1031 - 1081 (NASA)	0.015 - 0.017
585 - 650 (LASL)	0.070 - 0.076

Crystals were grown by an unseeded, closed tube sublimation method used for manufacturing lasers at Laser Analytics, Inc. The general growth techniques have been described in detail for $Pb_{1-x}Sn_xSe$ in a publication by Harman and McVittie. [13] Crystals are grown in a sealed quartz ampoule from a previously reacted and purified polycrystalline source using a small, carefully maintained temperature gradient. The polycrystalline ingot crystallizes through the vapor phase, and crystals are formed directly

on the ingot without contacting the ampoule walls. The crystals generally exhibit well-faceted (100) surfaces with linear dimensions of 1-5 mm. The crystals are not purposely doped with impurities, but may grow either n- or p-type by controlling stoichiometry.

A total of thirteen growth runs were conducted specifically for determining the quality of lasers obtained from the lower temperature technique for defining the junction. These growths yielded 13 groups of crystals. Table 2.1 lists the growth runs, along with crystal dimensions and thermal probe data. Additional crystals used during the latter part of this program were selected from standard Laser Analytics production runs, and are described in the appropriate sections.

2.1.2 Characterization of $Pb_{1-x}Sn_xSe$ Crystals

The principle techniques used for evaluating the quality of the crystals grown for this contract were the following:

(a) visual inspection of the as-grown facets;

(b) etch pit density (EPD) measurements to estimate dislocation densities;

(c) surface etching followed by EPD measurements to determine the depth of damage effects.

These techniques are described in more detail below. Carrier concentration measurements were another important means of characterizing crystals since several laser parameters are expected to be related to this parameter. These measurements are described in sub-section 2.1.2.4.

2.1.2.1 Visual Inspection

The visual inspection technique has proven useful to evaluate the quality of as-grown facets. In particular, with careful use of side-lighting under a low power (10-20X), wide-angle microsope, it is

Table 2.1

Summary of PbSnSe Crystals Grown on This Contract

Growth No.	Comp X(%)	Description of Crystals		
		Bulk Material Type	Probe voltage (mV)	Crystal facet size range
GN-1	3.4	N	14	2-5 mm
GN-2	1.6	N	14	1-3 mm
GN-3	3.4	N	23	3-5 mm
GN-4	1.6	N	20	2-4 mm
GN-5	1.6	N	10	2-4 mm
GN-6	3.4	N	16	2-3 mm
GN-7	7.2	N	14	2-4 mm
GN-8	7.0	N	14	2-5 mm
GN-9	7.2	N	16	2-3 mm
GN-10	7.4	N	12	2-3 mm
GN-11	3.2	N	17	2-5 mm
GN-12	3.2	N	10	2-5 mm
GN-13	1.6	P	29	2-3 mm

Notes: (1) The thermal probe voltages were obtained with a hot-tip temperature of 150°C. These data were later correlated with Hall data as described in table 2.2. The carrier concentration values can be deduced from Figure 2.4.

(2) Approximately 2 to 3 usable crystals were obtained from each of the above growth runs. The dimensions given are those describing the largest crystals from each run.

possible to observe the presence of defects such as small angle grain boundaries. Crystals with excessively high numbers of defects were rejected. The crystals used in this work all had observable defect densities of less than approximately one per 6 mm^2. With such a low density of gross defects, the odds of fabricating lasers from a grain boundary region (such regions are impossible to identify after the crystal wafers have been metallized) are very small.

2.1.2.2 Etch Pit Density Measurements

Etch pit density (EPD) measurement has proven to be an effective and simple technique for determining dislocation densities in Pb-salt crystals. Such measurements were made by preparing an etch of the following composition:

10 gm KOH
10 ml H_2O
1 ml glycerol
0.5 ml H_2O_2

and using this solution at room temperature for 1-2 minutes. The EPD measurement is then made by counting the number of etch pits in a known area within the field of view of a microscope. Such EPD values are usually not uniform over an entire crystal facet; some wafers exhibit high EPD regions and other regions with no etch pits at all. Averaged over the entire crystal facet, our EPD measurements on as-grown facets were usually in the 10^4 cm^{-2} range. Values below 10^4 cm^{-2} are considered good for Pb-salt crystals.

2.1.2.3 Etch Pit Density Measurements of Surface Etched Crystals

EPD measurements as a function of depth below the surface of as-grown facets have been made on $Pb_{1-x}Sn_xSe$ crystals. The appearance of such a crystal (G290) which had been etched in KOH for several minutes is shown in Figure 2.1. Once a certain etch-depth was reached, this type of appearance was observed no matter how deep the sample was then etched. Prior to reaching a depth where this type of bulk morphology was observed, however, it was found that the surface morphology was quite different. To

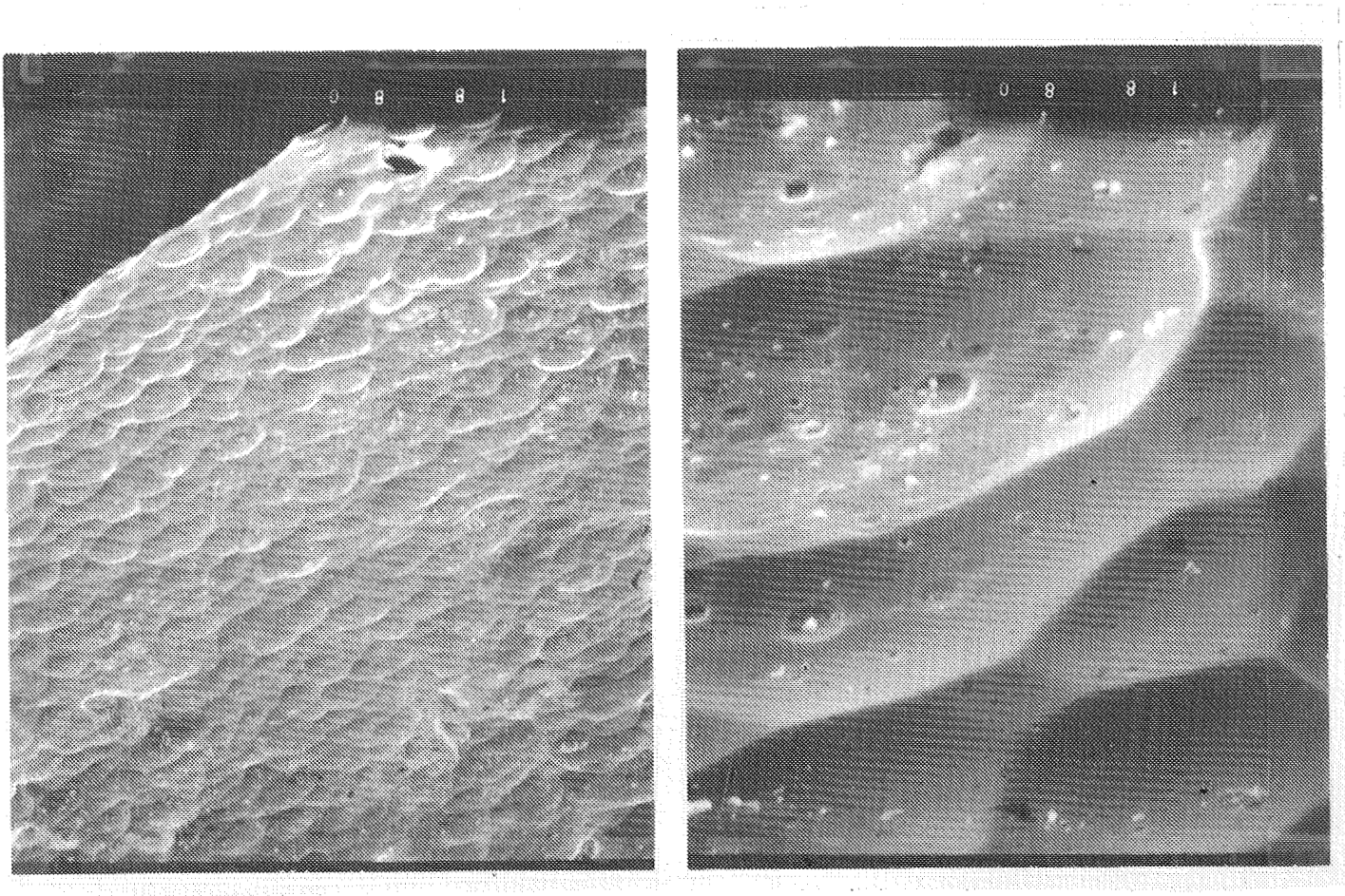

Figure 2.1

SEM photographs of a PbSnSe crystal after a few μm of material had been removed by the KOH etch. Left magnification = 300X, right magnification = 3000X. Crystal studied was G290, composition $Pb_{.975}Sn_{.025}Se$ with a thermal probe- deduced, n-type carrier concentration of 4 x 10^{19} cm^{-3}.

an etch depth of less than 1 μm below the facet, it was found that a rather nondescript, rough looking surface occurred. Further etching revealed a transition to the bulk appearance shown in Figure 2.1. The appearance of the crystal morphology at the transition between the initial etch region to the bulk etch region is shown in Figure 2.2. The 3000X magnification photograph of this figure shows the remaining residue of what almost appears to be a surface crust whose removal brings the surface to its bulk morphological condition. This phenomenon was observed with several other crystals besides G290.

In order to better understand the depth-distribution of dislocation densities, etch pit density measurements were made on both as-grown facets and on bulk material with the surface region removed by KOH etching. A comparison of the EPD for identical regions of the crystal both before and after etching to a depth of several μm is shown in Figure 2.3. The left photo shows the as-grown facet with the EPD of approximately 6×10^3 cm^{-2}, while the same region, when KOH-etched to remove several μm of material shows an EPD of approximately 1.2×10^3 cm^{-2}. It is clear that the bulk material seems to have a lower EPD value than the surface region of the crystal.

The results of the EPD measurements suggest that the surface regions of as-grown Pb-salt crystals may be heavily damaged, to a depth of approximately 1 μm. An important conclusion is that CID heterojunction and pn-junction depths should be substantially below this depth. The damaged region may play a role in contact degradation, although this possibility was not investigated in the present study.

2.1.2.4 Carrier Concentration Measurements

Knowledge of the type and concentration of charge carriers is important for, among other reasons, forming pn-junctions at desired and reproducible depths. The purpose of the experiment described in this subsection was to calibrate a thermal probe against Hall measurement data. Use of a calibrated thermal probe allows small irregular samples to be characterized with relative ease, and has other uses mentioned below.

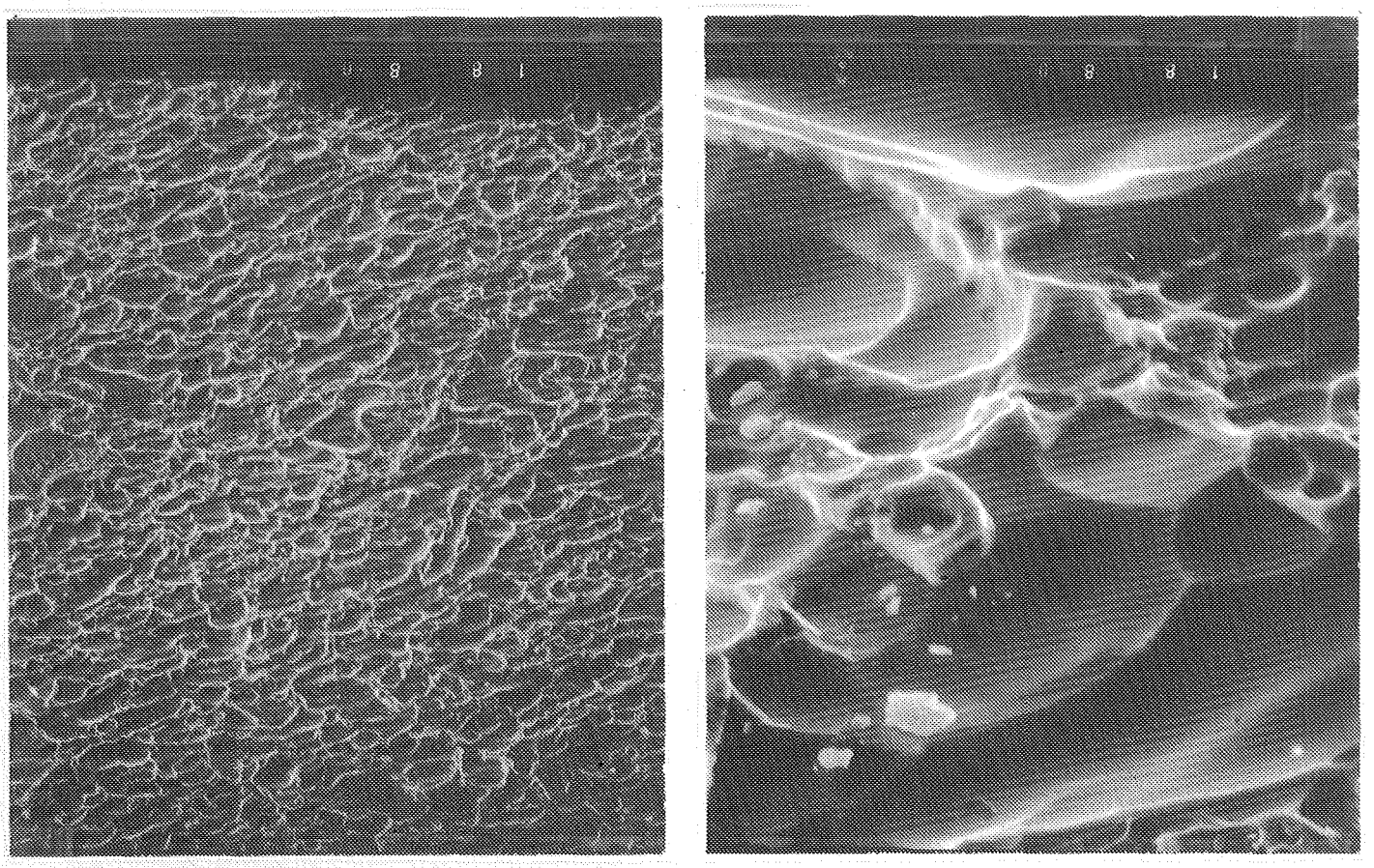

Figure 2.2

SEM photographs of the same crystal taken just before a depth was reached which had the characteristics of the bulk material. At this point, approximately 1 μm of material has been removed, and the 3000X (right) photograph shows evidence of a surface crust which is just beginning to be removed by the KOH etch. Left photo = 300X.

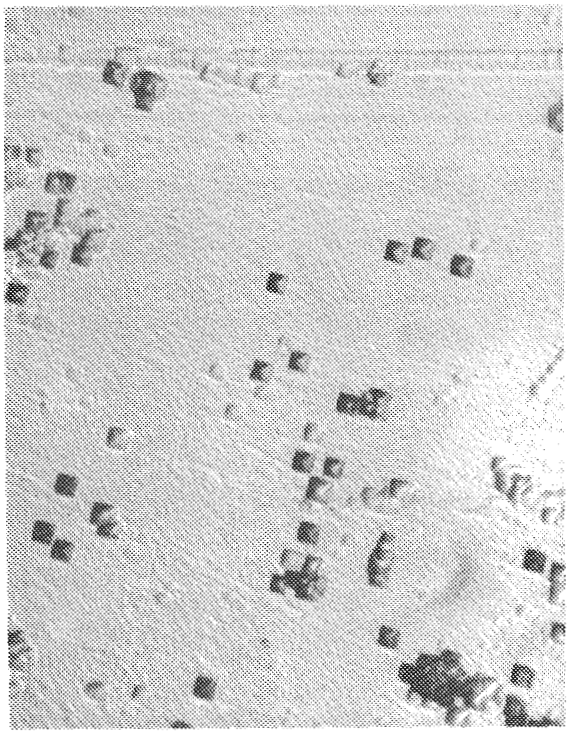

UNETCHED

ETCHED

CENTER OF FACET

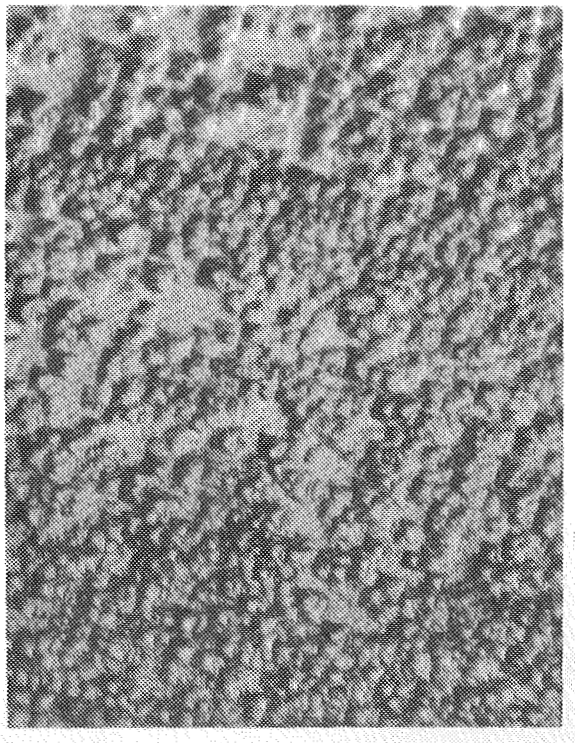

UNETCHED

ETCHED

EDGE OF FACET

Figure 2.3

EPD measurements carried out on an as-grown facet (left photos) and then on bulk material several μm below the facet surface following the removal of surface material by the KOH etch (right photos). The sample area shown in the photographs is approximately 6 x 10^{-3}cm^2.

Carrier concentrations of semiconductor crystals are most accurately measured from the Hall effect, using a technique described by Van der Pauw, (14); the samples are thinned to a uniform thickness of approximately 1/2 mm and 4 soldered In contacts are made at random locations at its edges. Van der Pauw samples were prepared from several $Pb_{1-x}Sn_xSe$ crystals. The Van der Pauw sample Hall data were then used as standards to calibrate our thermal probe. The thermal probe, based on the Seebeck effect in which a heated contact wire causes a thermo-electric voltage to occur between the wire and the sample, was found to be a convenient tool for determining the carrier concentration of as-grown crystals, surface carrier concentrations of diffused samples, and to determine p-n junction locations. The calibration data obtained for the thermal probe are shown in Table 2.2. These same data are plotted as thermal probe voltage vs. measured carrier concentrations in Figure 2.4. This figure then provided calibration data for our carrier concentration measurements using the thermal probe. Note that the data points are limited to an accuracy of approximately 10%. It was found that on bulk samples the thermal probe voltages were nearly the same after the samples were etched down several μm below the facet surface, indicating no measurable changes in carrier concentration. Similarly, in the case of diffused samples, it was found that the thermal voltages remained nearly constant until within approximately a μm of the junction region, where they abruptly changed to the bulk value.

2.1.3 Formation and Investigation of p-n Junctions

Formation of p-n junctions and, more generally, control of carrier type and concentration in the Pb-salts are based on controlling deviations from the stoichiometric ratio of 1:1 for the metal and non-metal constituents. Effects related to stoichiometry deviations in the Pb-salts are quite large, in contrast to the case for the III-V compounds, in which such effects only come into play at very low carrier concentrations. The diffusion processing for forming p-n junctions in the Pb-salts can be described by an interdiffusion constant whose value depends on the substrate carrier type and concentration as well as temperature and other factors.

Table 2.2

Calibration Data for Thermal Probe Voltages
Obtained from Van der Pauw Samples of $Pb_{1-x}Sn_xSe$

Sample of $Pb_{1-x}Sn_xSe$	x	Carrier Concentration as determined by Hall Measurements at 300 K (cm^{-3})	Carrier Concentration as determined by Hall Measurements at 77 K (cm^{-3})	Laser Analytics Thermal Probe Reading (mV) for 150°C Hot Tip
G154	.038	P 3.86×10^{18}	P 6.23×10^{18}	+23
G88	.067	P 1.04×10^{19}	P 1.36×10^{19}	+19
G232	.047	N 1.33×10^{19}	N 1.34×10^{19}	-25
G231	.055	N 3.4×10^{19}	N 3.8×10^{19}	-10
G225	.070	N 2.8×10^{19}	N 2.42×10^{19}	-12
G223	.070	N 2.8×10^{19}	N 3.17×10^{19}	-10
G344	.047	N 1.6×10^{18}	N 1.5×10^{18}	-38

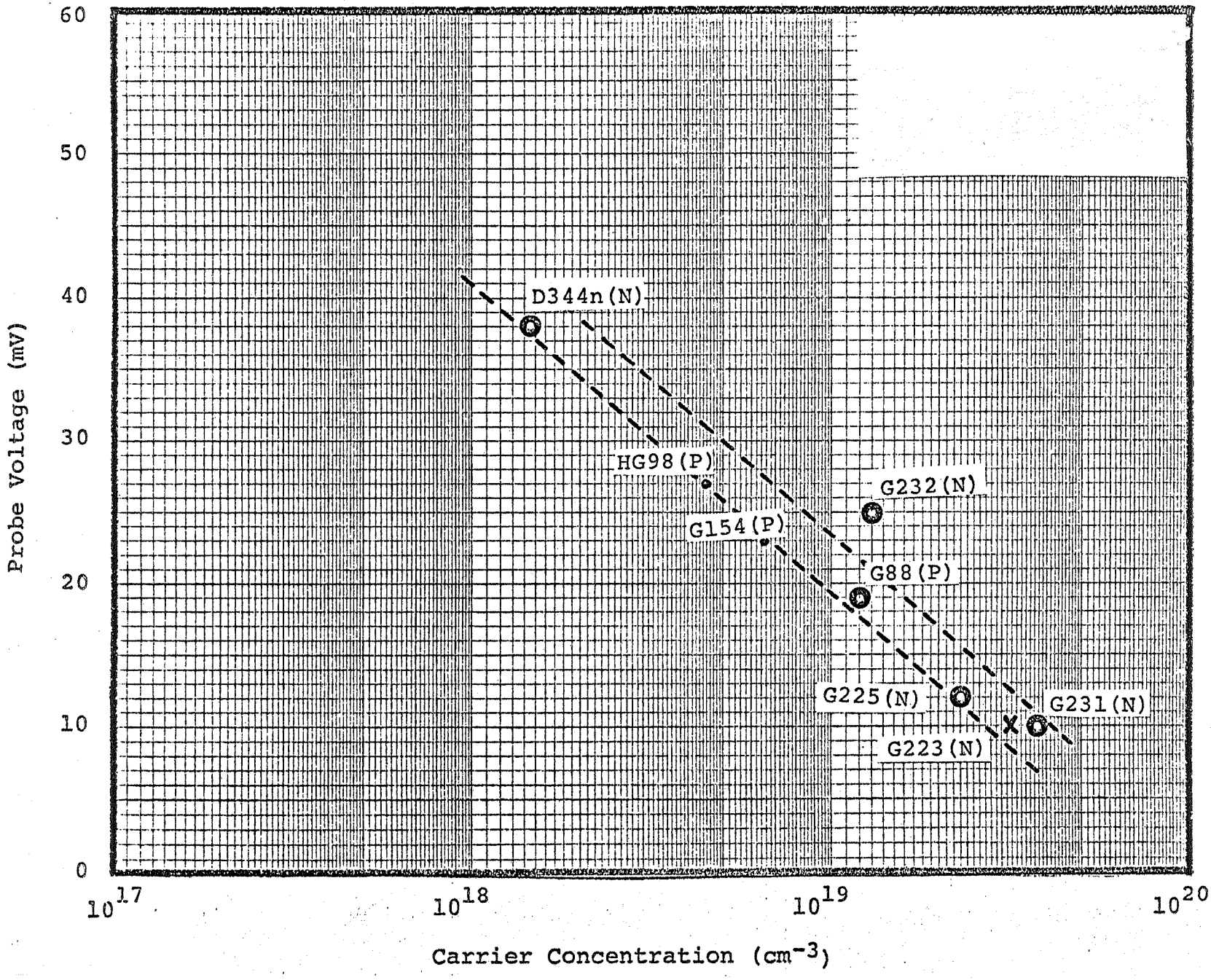

Figure 2.4

Thermal probe voltages vs. carrier concentration values obtained from Van der Pauw measurements for $Pb_{1-x}Sn_xSe$ at room temperature. Sample D344n was specially annealed to obtain this reduced carrier concentration.

Junction depth studies were carried out on p-type and n-type PbSnSe for several compositions between x = 0.034 and x = 0.070. Junction depths were measured by a step-etch technique, with the height of each step being measured by focusing a high power metallographic microscope alternately on the unetched and etched surfaces, giving a resolution of approximately 2 μm. A summary of thermal probe/step-etch data is given in Table 2.3. The p-n junction position was located at the depth at which the Seebeck voltage changed sign.

P-n junctions were formed by the standard techniques used in the production of PbSnSe diode lasers. Crystals were sealed in evacuated quartz ampoules with vapor sources consisting of 1% metal, or Se-rich charges. Diffusions were performed for a variety of time-temperature conditions. At the end of each run, the ampoules were air quenched and opened under vacuum.

It was found that for n diffusions into p materials, junction depths varied widely for fixed diffusion parameters. For example, a series of production runs at 600°C for 20 minutes produced junction depths ranging from less than 1 μm to more than 30 μm, with most junction depths between 3 μm and 10 μm. For p into n diffusion, on the other hand, consistent reproducible results were obtained. Similar results for diffusions into PbSe have been reported by researchers at M.I.T. Lincoln Laboratory; (2) they ascribed the variability of results for n into p diffusions to surface effects which produce an effective diffusion barrier. While this variability is a significant factor and must be accounted for in the manufacturing process, attempts to study and solve the problem were beyond the scope of the present program.

For p into n diffusions, reproducible and meaningful results were achieved and were analyzed as follows. An effective diffusion coefficient, D, was calculated, assuming that the diffusion process obeys a Fick's Law relationship:

$$\Delta = \Delta_0 \operatorname{erf} \frac{x}{2\sqrt{Dt}} \qquad (4)$$

Table 2.3

Crystal GN-No.	Crystal Comp. (X)	n-Type Carrier Concentration (cm^{-3})	Diffusion Temp./Time (°C)/(hrs.)	Measured Junction Depth (μm)	Estimated Diffusion Coefficient (Fick's Law) ($cm^2 sec^{-1}$)
6	0.34	2.1×10^{19}	400/1	5	6.94×10^{-11}
8	0.070	2.3×10^{19}	400/1	8	1.78×10^{-10}
8	0.070	2.3×10^{19}	375/1	5.5	8.4×10^{-11}
7	0.072	2.3×10^{19}	400/1	8	1.78×10^{-11}
7	0.072	2.3×10^{19}	400/1	9	2.25×10^{-10}
7	0.072	2.3×10^{19}	450/1	22	1.34×10^{-9}
7	0.072	2.3×10^{19}	500/1	58	9.34×10^{-9}

Junction Depths for p-type Diffusions into n-type $Pb_{1-x}Sn_xSe$ as Measured by a Thermal Probe/Step Etching Technique. Diffusion Coefficients Were Estimated Assuming a Fick's Law Relationship.

where Δ is the deviation in carrier concentration from the equilibrium value Δ_0, x is the distance into the material, and t is the time for locating the 50% tail into the bulk material (or, approximately the junction depth) $D = x^2/t$. If we assume that diffusion coefficient has the form:

$$D = D_0 \exp(-\Delta E/kT) \text{ cm}^2 \text{ sec}^{-1}, \tag{5}$$

then it is possible to plot D_0 vs. ΔE for each of the diffusions (since D is known at a fixed value of T). Such plots for crystals GN-7 and GN-8 are shown in Figure 2.5. If we assume that D_0 is nearly independent of composition, then the region where D_0 is nearly the same for all samples corresponds to a value of $D_0 = 10^2$ cm^2 sec^{-1} and $\Delta E = 1.5$ eV.

The diffusions represented by these plots are for 375°, 400°, 450° and 500°C, all for material with x = 0.070 or 0.072. Thus the diffusion coefficient for this material has the form:

$$D = 1 \times 10^2 \exp(-1.5/kT) \text{cm}^2 \text{ sec}^{-1}. \tag{6}$$

This relationship is useful in predicting junction depths for p-skin formation in n-type crystals of $Pb_{1-x}Sn_xSe$. All diffusions during the first part of the program were carried out on material with 50 μm wide stripes in which the insulator material was also used as the diffusion masking material. A summary of the diffusion carried out during the first 6 months of the program is given in Table 2.4. The post-diffusion thermal probe voltages indicate near-surface carrier concentration of the order of 10^{18} cm^{-3}. Such high values are considered desirable in obtaining low values of contact resistance.

2.1.4 Fabrication of $Pb_{1-x}Sn_xSe$ Lasers

Lasers were fabricated for this program using the standard Laser Analytics manufacturing facilities and methods. The laser dice, after metallization, were installed in the standard heat sink package, using In bonding techniques.

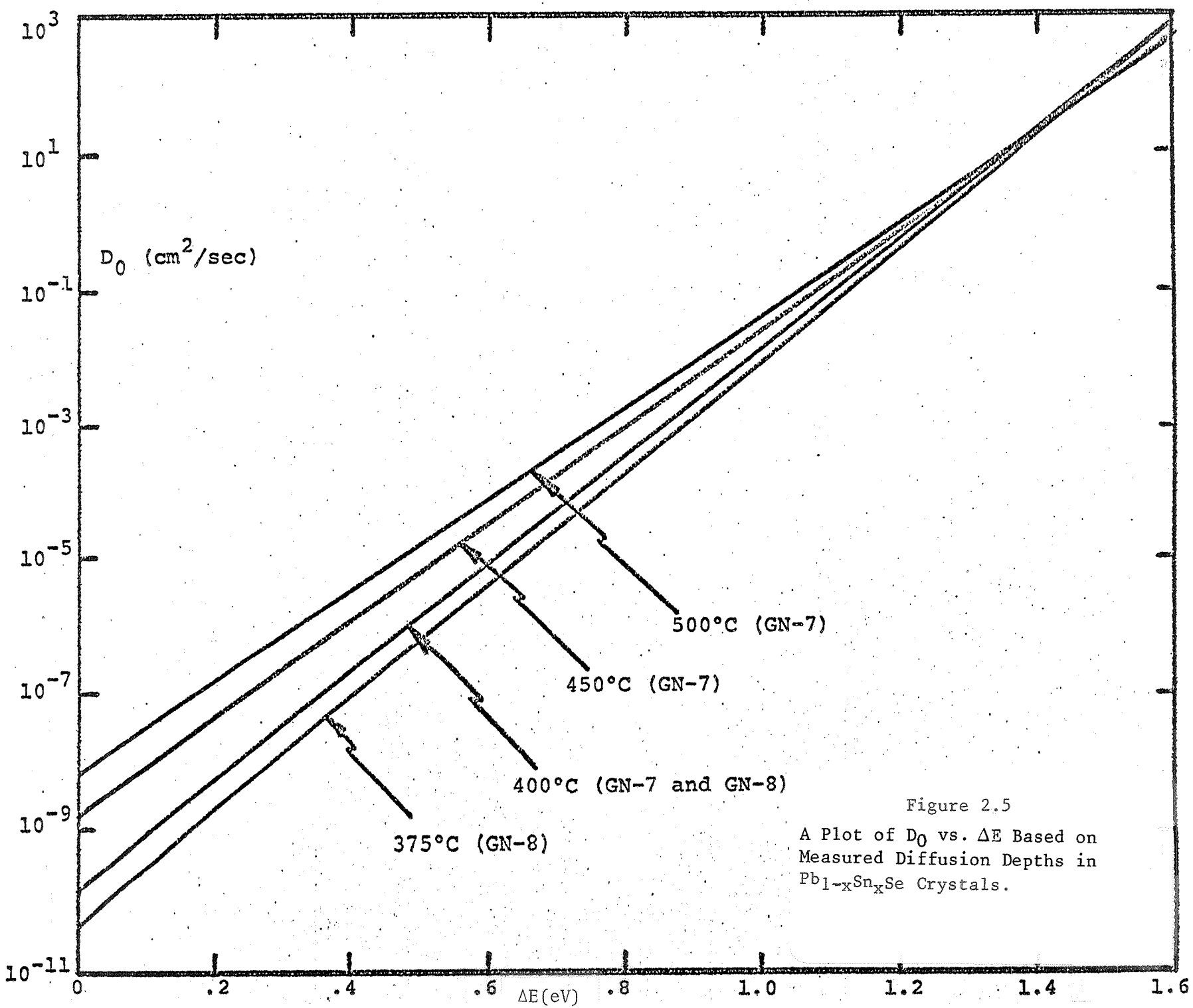

Figure 2.5

A Plot of D_0 vs. ΔE Based on Measured Diffusion Depths in $Pb_{1-x}Sn_xSe$ Crystals.

Table 2.4

Summary of Diffusion Runs for Crystals Grown on this Contract

Diffusion Run	Date Diffused (1978)	Crystal No.	Compos. (x)	Diffusion Temperature (°C)	Indicated Surface Carrier Concentration (cm^{-3})*
DN-1	1/25	GN-5	.016	400	1.2E19
DN-2	1/25	GN-1	.034	400	3.5E19
DN-3	1/27	GN-4	.016	400	7.8E18
DN-4	1/31	GN-8	.070	400	1.0E19
DN-5	2/13	GN-1	.034	400	5.0E19
DN-6	2/14	GN-6	.034	400	5.0E19
DN-7	2/14	GN-7	.072	400	5.0E19
DN-8	2/17	GN-4	.016	400	1.5E18
DN-9	2/21	GN-1	.034	400	7.0E18
DN-10	3/3	GN-9	.072	400	2.3E19
DN-11	3/23	GN-1	.034	425	3.2E18
DN-12	3/23	GN-8	.070	400	2.3E19
DN-13	3/23	GN-4	.016	400	1.7E18
DN-14	3/24	GN-9	.072	400	1.4E19
DN-15	3/28	GN-1	.034	400	3.5E19
DN-16	4/4	GN-6	.034	400	3.5E19
DN-17	4/11	GN-1	.034	425	3.6E18
DN-18	4/11	GN-6	.034	425	6.2E18
DN-19	4/12	GN-1	.034	425	4.0E18
DN-20	4/18	GN-1	.034	400	2.1E19
DN-21	4/18	GN-1	.034	400	2.0E19
DN-22	4/18	GN-1	.034	400	7.0E18
DN-23	4/27	GN-3	.034	425	5.0E19
DN-24	5/26	GN-9	.072	425	3.7E19
DN-25	6/6	GN-12	.032	425	1.0E19

*Estimated Accuracy ± 25%

Notes: (1) All diffusions listed above were carried out for 1 hour.
(2) Junction depths not measured but were estimated to be approx. 7 ± 2 μm for the 400°C diffusion and 12 ± 2 μm for the 425°C diffusion.

Crystals were selected for highest quality in terms of few or no grain boundaries and etch pit densities below 10^5 cm^{-2}. Early in the program, it was discovered that lasers formed with p-skin, n-bulk material were generally poor in all respects and would not meet contractual specifications. Specifically these lasers, fabricated from runs DN9, 12, 16, 21 and 25, generally had low output power values and exhibited significant degradation in contact resistance after 1-3 months. Deliverable lasers for the program were all fabricated from n-skin, p-bulk crystals.

In order to obtain desired junction depths for the n-skin, p-bulk crystals, samples were cleaved off for thermoprobe evaluations. Lasers were generally fabricated from samples with junction depths of 10 μm or less.

A number of lasers were fabricated in the early stages of this program using n-bulk crystals. These units exhibited increases in the electrical contact resistance over a few months of shelf storage under ambient temperature conditions. While such lasers still operated after periods of 150 days, their increased contact resistance values were expected to lead to increased tuning rates and eventually complete failure. In some cases, the observed degradation behavior occurred after shelf storage periods as short as 1600 hours (2 months). As will be seen in Section 2.2, this degradation is associated with metal-to-semiconductor contact phenomena.

Later attempts to produce high quality lasers, using improved techniques, were successful and a total of sixteen lasers were assembled, characterized and delivered. These lasers will be described in detail in a later section.

2.2 Diode Laser Degradation and Failure

2.2.1 Shelf Storage Degradation

As discussed in the introduction, the shelf storage degradation was in many respects one of the most critical problems in $Pb_{1-x}Sn_xSe$ laser technology. This subsection describes a series of experiments aimed at characterizing and defining the problem and the use of techniques which have greatly reduced its severity.

2.2.1.1 Low Temperature Storage

It was believed that the increase in contact resistance with time was temperature dependent and did not occur at cryogenic temperatures. To test this hypothesis a laser was stored for 9 months in a sealed glass tube immersed in liquid nitrogen. Results are summarized in Figure 2.6 which shows the IV characteristics of the laser before and after storage. The data are summarized as follows:

Initial		After 9 months of continuous storage at liquid nitrogen temperature	
$R_f(\Omega)$	I_{th}(mA)	$R_f(\Omega)$	I_{th}(mA)
.0210	355	.0215	520

Several other lasers fabricated from this same run exhibited increases in resistance of approximately .1 ohms after storage at room temperature for only a few weeks. It appears that low temperature storage greatly improves the contact stability of otherwise unstable devices. The increase in threshold current without a corresponding increase in leakage current (defined earlier) is believed to be an anomaly since such an effect is not generally observed in lasers stored at room temperature, whether degraded or not.

2.2.1.2 Analysis of Degraded Production Lasers

Laser Analytics has maintained a log of the properties and history of all lasers manufactured by the company during its existence. These data provide a useful base to characterize shelf storage degradation for a large number of devices.

Data on both electrical and optical characteristics of 116 $Pb_{1-x}Sn_xSe$ diode lasers fabricated from a total of 45 different diffusion runs over a 1-1/2 year period (mid 1976-1977) were measured at various time intervals after laser assembly. These data have been compared to those taken immediately after laser assembly. The specific data of interest are the following:

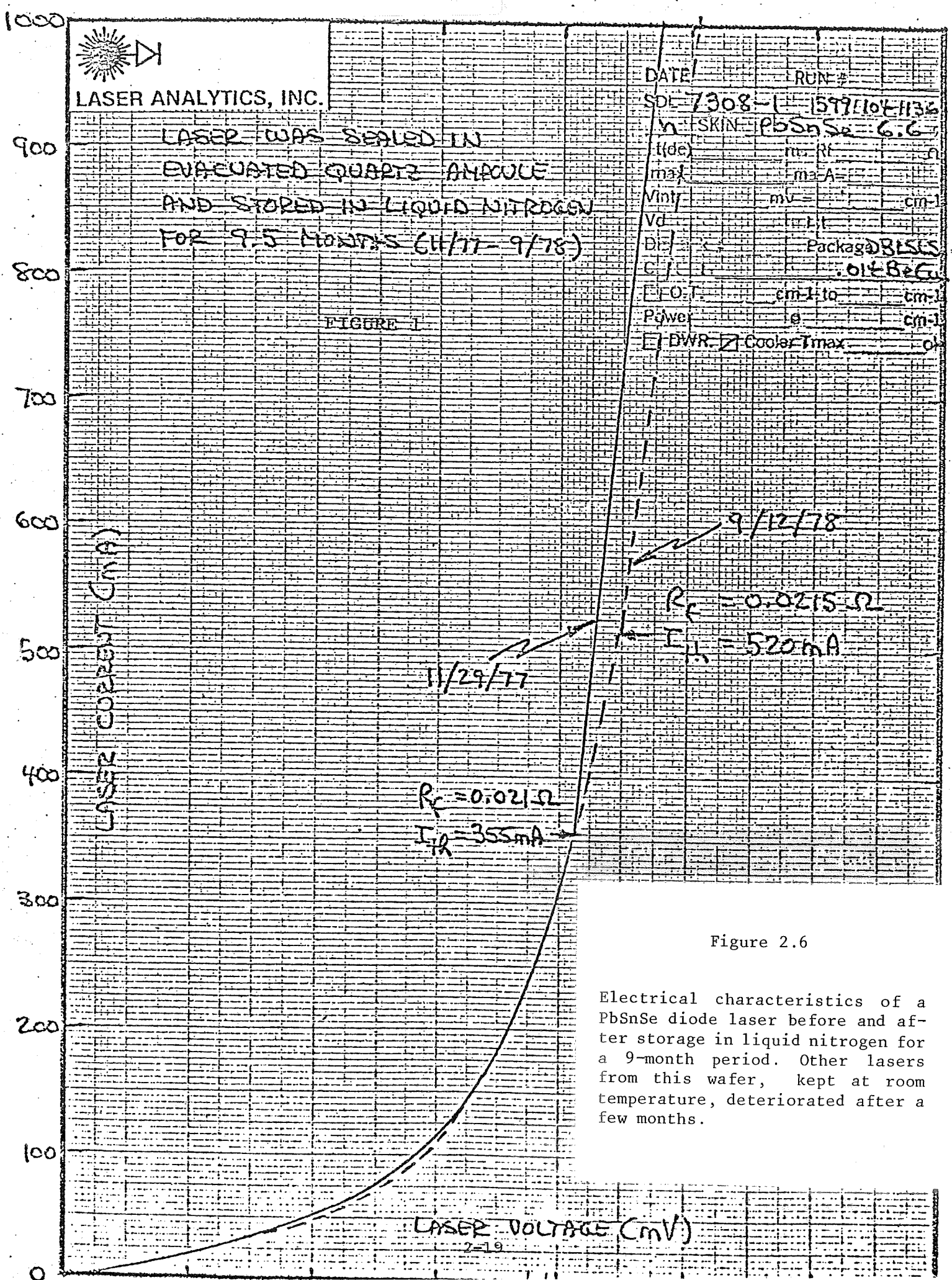

Figure 2.6

Electrical characteristics of a PbSnSe diode laser before and after storage in liquid nitrogen for a 9-month period. Other lasers from this wafer, kept at room temperature, deteriorated after a few months.

a. Threshold current, the current at which the laser begins to emit laser radiation.
b. Forward-bias resistance, inverse slope of the I-V curve at just above threshold.
c. Leakage current (defined as that current measured at a forward-bias voltage which is half that of the intercept voltage, i.e., half that obtained on the voltage axis at which a line drawn tangent to the I-V curve right above threshold intersects the axis).
d. Detector saturation current, defined as that value of laser current for which the Ge:Cu detector voltage saturates. The difference between this value and the threshold current gives an indication of the relative laser output power. When the detector saturation current is less than about 120% of the threshold current, the lasers generally have good output levels (>.25 mW).
e. Maximum allowable laser current (the current above which the I-V product exceed approximately 0.5 Watts) often indicates the relative heating that occurs and can sometimes be related to the thermal resistance of the laser, although for high contact resistance values, this may be misleading.

Comparative data on these 116 $Pb_{1-x}Sn_xSe$ lasers studied during this time period were compiled by an HP9825A computer and are presented in Table 2.5. This table presents average values of the changes in the above parameters observed over periods of time whose average values (in days) are shown in the extreme right column. Standard deviations are also shown in order of decreasing SnSe concentration. Thus, lasers with the high SnSe values indicate long wavelength devices (~25-30 μm) while lasers with low SnSe values indicate shorter wavelengths (approximately 9 μm for 0.4%).

Summary of diode laser changes after specified periods of shelf-storage time, covering mid 1976-1977. Entries are in order of increasing diffusion run numbers.

DIFFUSION		MATERIAL	NO. OF LASERS	CHANGE IN THRESHOLD CURRENT (mA)		CHANGE IN FORWARD RESISTANCE (ohms)		CHANGE IN LEAKAGE CURRENT (mA)		CHANGE IN CURRENT FOR DETECTOR SATURATION (mA)		CHANGE IN MAX. ALLOWABLE LASER CURRENT (mA)		TIME BETWEEN TESTS	
RUN NO.	TEMP. (°C)	COMP/TYPE		AVE.	σ	AVE.	σ	AVE.	σ	AVE.	σ	AVE.	σ	AVE.	σ
273	600	21.0PbSnSe	1	10	0	0.02	0.00	10	0	-25	0	0	0	8	0
564	600	10.0PbSnSe	2	-48	18	0.00	0.00	-10	0	-155	55	0	0	14	0
483·	400	7.8 PbSnSe	7	69	369	0.13	0.18	-56	67	411	1025	-57	232	79	31
700·	450	7.0 PbSnSe	2	35	65	0.01	0.01	-24	19	-50	50	0	0	25	0
558	500	7.0 PbSnSe	1	0	0	0.03	0.00	0	0	0	0	0	0	33	0
556·	400	7.0 PbSnSe	2	48	10	0.07	0.04	15	0	225	25	-150	150	38	23
168	600	6.9 PbSnSe	4	366	383	0.13	0.15	-21	17	304	378	-388	562	57	27
170	600	6.7 PbSnSe	2	-448	597	0.04	0.01	8	2	-825	725	-200	0	73	27
439	600	6.6 PbSnSe	2	106	50	0.04	0.03	0	5	825	25	0	0	86	83
619	600	6.6 PbSnSe	3	332	157	0.18	0.09	-37	52	883	272	-400	283	56	6
599	550	6.6 PbSnSe	2	-560	425	0.02	0.01	-18	18	-15	85	0	0	39	38
450	500	6.6 PbSnSe	3	20	36	0.02	0.02	13	13	-13	26	-67	94	41	26
440	550	6.6 PbSnSe	1	-65	0	0.00	0.00	-50	0	-100	0	0	0	9	0
664	600	6.5 PbSnSe	3	-44	48	0.11	0.09	-10	14	-83	165	0	0	30	21
448	600	6.5 PbSnSe	1	225	0	0.08	0.00	-5	0	400	0	0	0	80	0
605	550	6.0 PbSnSe	3	473	398	0.05	0.03	-48	47	225	336	-67	94	42	15
143	600	6.0 PbSnSe	5	425	385	0.09	0.07	-11	20	628	558	-320	271	268	83
658·	400	5.5 PbSnSe	1	-255	0	0.15	0.00	-160	0	-190	0	0	0	58	0
189	600	5.0 PbSnSe	1	-285	0	0.03	0.00	0	0	-350	0	0	0	79	0
184	600	5.0 PbSnSe	1	-45	0	0.01	0.00	20	0	300	0	0	0	28	0
709	600	4.7 PbSnSe	1	75	0	0.00	0.00	22	0	300	0	0	0	26	0
669	600	4.7 PbSnSe	2	-34	28	-0.01	0.01	0	5	63	163	0	0	39	18
286	600	4.7 PbSnSe	3	85	235	0.02	0.04	-52	115	90	233	-300	245	110	8
201	600	4.7 PbSnSe	8	187	392	0.02	0.02	-46	153	476	522	0	0	96	118
312·	400	4.7 PbSnSe	4	295	376	0.05	0.02	1	41	263	383	0	0	28	0

Table 2.5

DIFFUSION		MATERIAL	NO. OF LASERS	CHANGE IN THRESHOLD CURRENT (mA)		CHANGE IN FORWARD RESISTANCE (ohms)		CHANGE IN LEAKAGE CURRENT (mA)		CHANGE IN CURRENT FOR DETECTOR SATURATION (mA)		CHANGE IN MAX. ALLOWABLE LASER CURRENT (mA)		TIME BETWEEN TESTS	
RUN NO.	TEMP. (°C)	COMP/TYPE		AVE.	σ	AVE.	σ	AVE.	σ	AVE.	σ	AVE.	σ	AVE.	σ
334·	400	4.5 PbSnSe	1	610	0	0.04	0.00	10	0	600	0	0	0	47	0
186	600	3.6 PbSnSe	2	30	220	0.04	0.03	38	2	140	240	-500	500	55	7
659·	400	3.4 PbSnSe	3	-202	233	0.10	0.07	3	10	-267	309	0	0	32	23
531	500	3.2 PbSnSe	6	-41	472	0.03	0.04	4	16	-22	645	-217	285	41	9
729·	400	3.0 PbSnSe	1	25	0	0.26	0.00	0	0	25	0	-1000	0	23	0
469·	400	3.0 PbSnSe	6	26	74	0.00	0.08	-15	17	75	99	142	643	35	30
414·	400	3.0 PbSnSe	1	480	0	-0.00	0.00	5	0	450	0	0	0	16	0
287·	450	3.0 PbSnSe	1	50	0	0.09	0.00	10	0	0	0	0	0	42	0
258	600	3.0 PbSnSe	3	374	231	0.00	0.00	35	36	440	220	0	0	21	7
743·	400	2.8 PbSnSe	1	280	0	0.05	0.00	20	0	350	0	0	0	5	0
537	550	2.8 PbSnSe	1	115	0	0.28	0.00	-10	0	100	0	-800	0	36	0
579·	400	2.6 PbSnSe	5	30	188	0.02	0.04	-1	25	-14	147	-80	652	12	3
360·	400	2.6 PbSnSe	2	-153	122	0.09	0.01	-113	42	-60	40	0	0	26	0
188	600	2.6 PbSnSe	3	208	191	0.07	0.05	0	4	552	91	-167	236	184	98
613	550	1.5 PbSnSe	4	126	103	0.05	0.02	1	2	113	102	50	87	37	39
724	600	1.3 PbSnSe	2	-20	20	0.52	0.46	-5	1	25	25	-1050	350	14	2
663	600	1.1 PbSnSe	1	-290	0	0.06	0.00	10	0	-500	0	0	0	25	0
220	600	1.1 PbSnSe	3	642	286	0.05	0.02	-2	6	750	378	-133	189	50	16
494	550	0.6 PbSnSe	2	-48	182	0.01	0.01	5	25	-100	200	-100	100	46	6
493	550	0.4 PbSnSe	3	3	105	0.04	0.04	0	14	-92	31	-617	510	51	31

NOTE: All Run No's with a dot were n-substrates with a p-diffusion, while those with no dot were p-substrates with an n-diffusion.

Table 2.5 (continued)

There are, of course, different ways of presenting degradation data of this type. The present format was chosen because it is most likely to reveal significant differences due either to composition or diffusion temperature. As can be seen by examining both the "change in forward resistance" column and also in the "threshold current change" column, major composition effects are not apparent. A further analysis comparing the relative changes per unit time has not revealed any significant dependence upon composition, diffusion temperature, or whether the bulk material was p-type or n-type. Those run numbers with n-type bulk material are indicated with a dot next to the number in column 1 of Table 2.5.

It is interesting to note that, of the diffusion runs, which, on the average, exhibited decreases in threshold current with time, all but three were high temperature diffusions. This is consistent with a previous observation that many of the high performance diode lasers fabricated from material diffused at 600°C exhibited decreases in threshold current with time (even though their resistance increased with time). The decrease in I_0 is usually accompanied by an equal decrease in diode leakage current and is believed to be a surface effect. Improved stability of I_0 may require development of a surface passivation technique.

No particular correlation between detector saturation current change or leakage current change with diffusion temperature or composition appears apparent. All of the devices still functioned as lasers during the time intervals indicated. While some lasers were as old as 10 months, the average laser age was closer to 2 months.

2.2.1.3 Preliminary Contact Evaluation Studies

Prior to the present NASA support program; a series of contact studies was initiated on bulk crystals on n-type and p-type $Pb_{1-x}Sn_xSe$. These tests were continued under the current contract with the addition of other contact materials and a systematic study to determine the optimum material thickness, material combination, methods for deposition as well as the mechanisms contributing to contact failure.

During our initial study, dice with the same dimensions as diode lasers were cleaved from bulk crystals and metallized using techniques that were then currently used on our production lasers; In contacts were evaporated and plated to n-type dice, while evaporated Au followed by evaporated and plated In layers were applied to p-type samples. Control samples consisting of copper dice to which the same metal layers were applied were also tested. The sample and control dice were mounted in standard LAI laser packages.

The devices were tested immediately after fabrication by installing them in a dipstick and measuring their volt-ampere curves at a temperature near 4.2°K using a 4-lead (Kelvin) configuration. After test, the samples were stored at room temperature and re-evaluated at low temperatures from time-to-time thereafter.

The semiconductor samples initially exhibited linear, resistive V-I curves with low values of resistance. Over time, the resistance increased and the curves became sublinear at high currents, indicating significant heating. Eventually the contacts became open circuited. The metal control samples showed linear behavior with very low resistances (in the order of 0.1 milliohm) and remained unchanged within measurement error for the duration of the experiments.

Figure 2.7 shows results for two n- and p-type samples. Both types of crystal exhibit a rapid increase of resistance during an initial stage, followed by a slower, but very significant rise. The degradation is clearly much worse on the n-samples. Other samples exhibited the same general behavior although the degradation rates varied considerably.

The observation of strong degradation of In contacts on n-type material was unexpected. As discussed in Section 1.2, previous discussion and hypotheses had been based upon the belief that degradation of Pb-salt diode contacts occurred on the p-surface only.

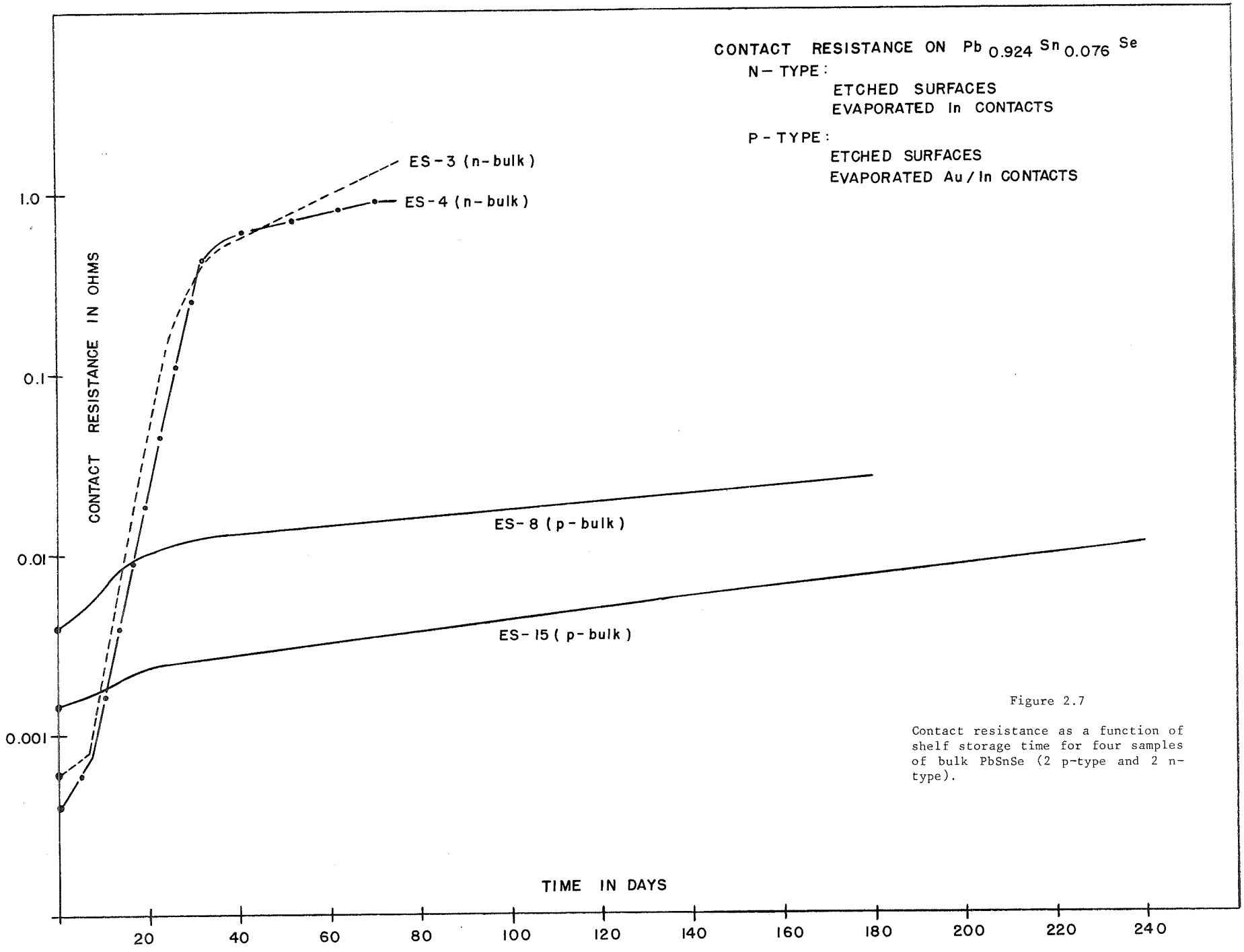

Figure 2.7

Contact resistance as a function of shelf storage time for four samples of bulk PbSnSe (2 p-type and 2 n-type).

In a related experiment, the carrier concentration stability of $Pb_{1-x}Sn_xSe$ was investigated by measuring the thermoprobe voltage of samples immediately after crystal growth and at intervals over a period of six months thereafter. The purpose was to test a hypothesis that the retrograde nature of the stability limits of $Pb_{1-x}Sn_xSe$ might lead to precipitation of metal or non-metal constituents in a crystal, and a corresponding effect on carrier concentration and therefore, sample resistance. Results summarized in Table 2.6, indicate no significant change in carrier concentration over the six month period. The variation on sample G-232 is believed to be due to a measurement error.

2.2.1.4 Auger Electron Spectroscopy (AES) Studies

A series of AES measurements was made on crystal surfaces which had been subjected to various processing treatments in an attempt to further understand the interface phenomena associated with contact degradation. AES is a powerful technique for semiquantitative measurements of trace elements on crystal surfaces. In conjunction with sputter-etching, it may be used to analyze subsurface regions, multilayer films and interface regions. Sputter-etch/AES measurements are limited in depth resolution to 100-200Å by redeposition, surface irregularities and other factors. Our measurements were performed by a local service firm, using a 5 KeV excitation beam; the work was supervised by members of the Laser Analytics staff.

A preliminary set of runs was carried out using a sample of $Pb_{0.972}Sn_{0.028}Se$ which had been subjected to a standard pre-metallization etch process. The spectrum is shown in Figure 2.8 and indicates the presence of bromine (a constituent of the etch) at a level of the order of 1 atomic % at the surface. A second spectrum obtained after a 10 second sputter etch (2 KV, 10 mA, estimated to remove approximately 10Å of material) confirmed the presence of bromine.

The final preliminary run utilized a sample ($Pb_{0.972}Sn_{0.028}Se$) metallized with a 2000Å layer of Au. An Auger depth profile was taken by sputter etching the sample while simultaneously tracing the lines

Table 2.6

Comparison of Thermoelectric Probe Data Taken on 6 Bulk Samples of $Pb_{1-x}Sn_xSe$ over a 6 Month Time Period. Variation Is Well Within Instrument Accuracy Except for Sample G232.

Sample No.	x Value	Thermoelectric Probe Voltage		Carrier conc. (as obtained from Van Der Pauw measurements) 3/78
		early 3/78	late 8/78	
D344 n	.047	-38	-37	1.6×10^{18} (N)
G154	.038	+23	+25	3.86×10^{18} (P)
G88	.067	+19	+16	1.0×10^{19} (P)
G232	.047	-25	-17	1.33×10^{19} (N)
G225	.070	-12	-13	2.8×10^{19} (N)
G231	.055	-10	-12	3.4×10^{19} (N)

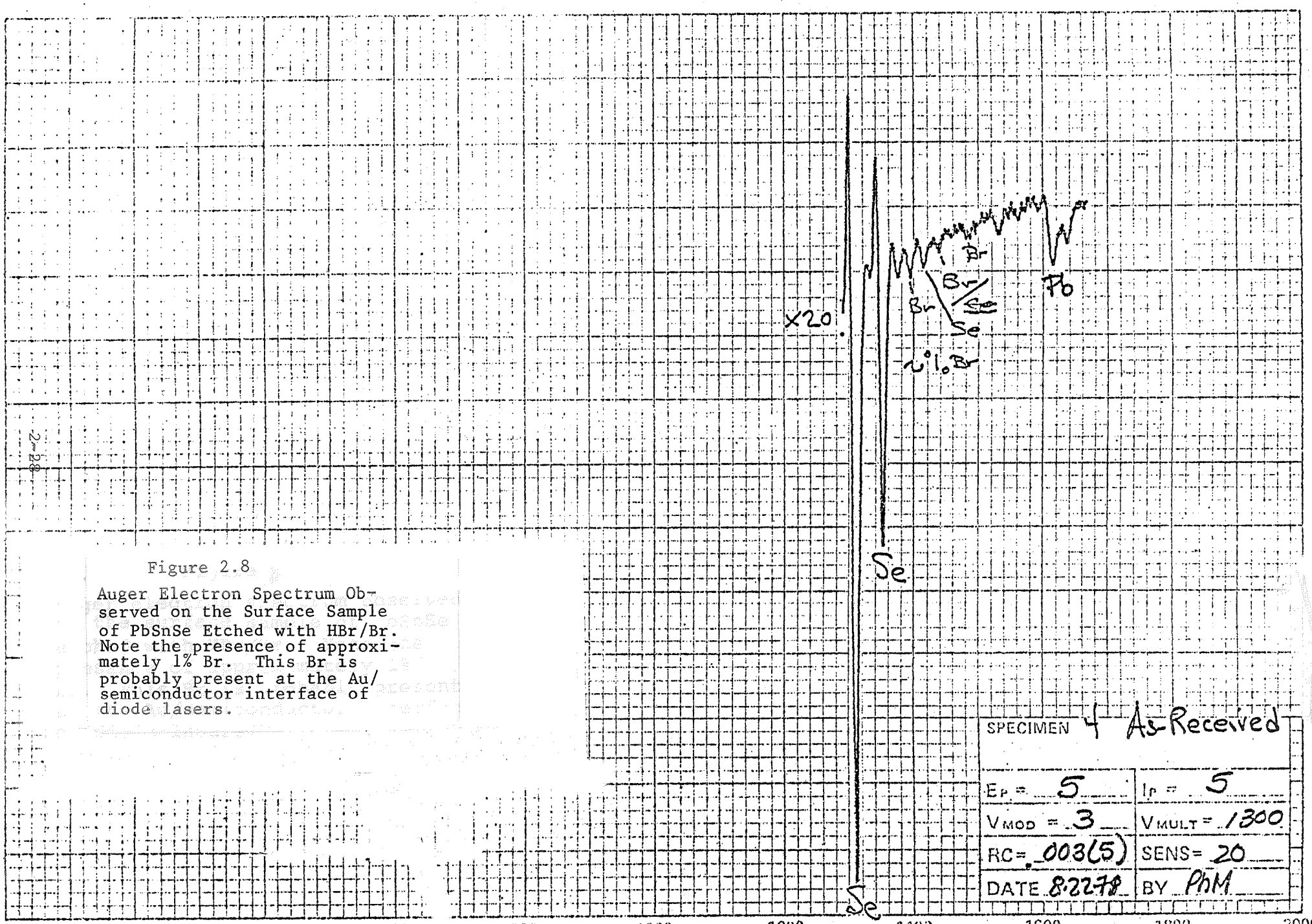

Figure 2.8

Auger Electron Spectrum Observed on the Surface Sample of PbSnSe Etched with HBr/Br. Note the presence of approximately 1% Br. This Br is probably present at the Au/semiconductor interface of diode lasers.

for Au, Se, O and C. The sputter etch rate was approxomately 40Å/min. (1 KV, 10 mA), and about 50 minutes were needed to remove the Au layer. The profile is shown in Figure 2.9. The apparent transition region width of about 200Å indicates the limit of resolution of the measurement. The lines shown for O and C correspond to the noise level of the signal, about 0.5 atomic %. Thus, any O or C at the interface is below this concentration.

In view of the fact that a major area to be investigated involved effects of room temperature migration and interaction of Au and In, there was particular concern about sample heating by the sputtering e-beam. Calculations indicated that the sample surfaces could easily be heated to 150-200°C unless precautions were taken. For this reason a cooling stage was developed which consisted of a standard sample holder to which a liquid nitrogen heat exchanger was attached. Without sputtering power, the sample temperature was about 100K.

In the next series of samples, wafers at various stages in the production process were analyzed using the cooled sample holder. Results indicated the presence of relatively large quantities (from 1 to 20 atomic %) of O, C, N, Cℓ and S on all samples. However, further investigation and analysis of additional crystals led to the conclusion that these elements originated from contamination, tentatively by the AES instrument; the contamination problem was believed to be exacerbated by cooling the samples since, being the coldest surfaces in the vacuum system, they were sinks for residual vapor and any material outgassed from surrounding surfaces. It was found that all samples which had been treated with a Br-based etch (and only those samples) exhibited barely measurable quantities of Br on their surfaces.

A final series of AES measurements was performed using three wafers; one that had undergone the then standard metallization and diffusion process, and two wafers having a few hundred Å of chromium as a "barrier" metal. Two of the wafers incorporated 50 μm stripes delineated with a CaF_2 insulator on the diffused side. Metallization was uniformly deposited over insulator and crystal.

PHYSICAL ELECTRONICS INDUSTRIES, INC.

SPECIMEN 2 Pg 1.

Element		Etching	
1	= Au x 5	Gun	1 / 2
2	= Se x 10		1 Ep
3	= O x 10		10 Ie
4	= C x 5	Rate:	40 Å/Min. Au
5			
6			

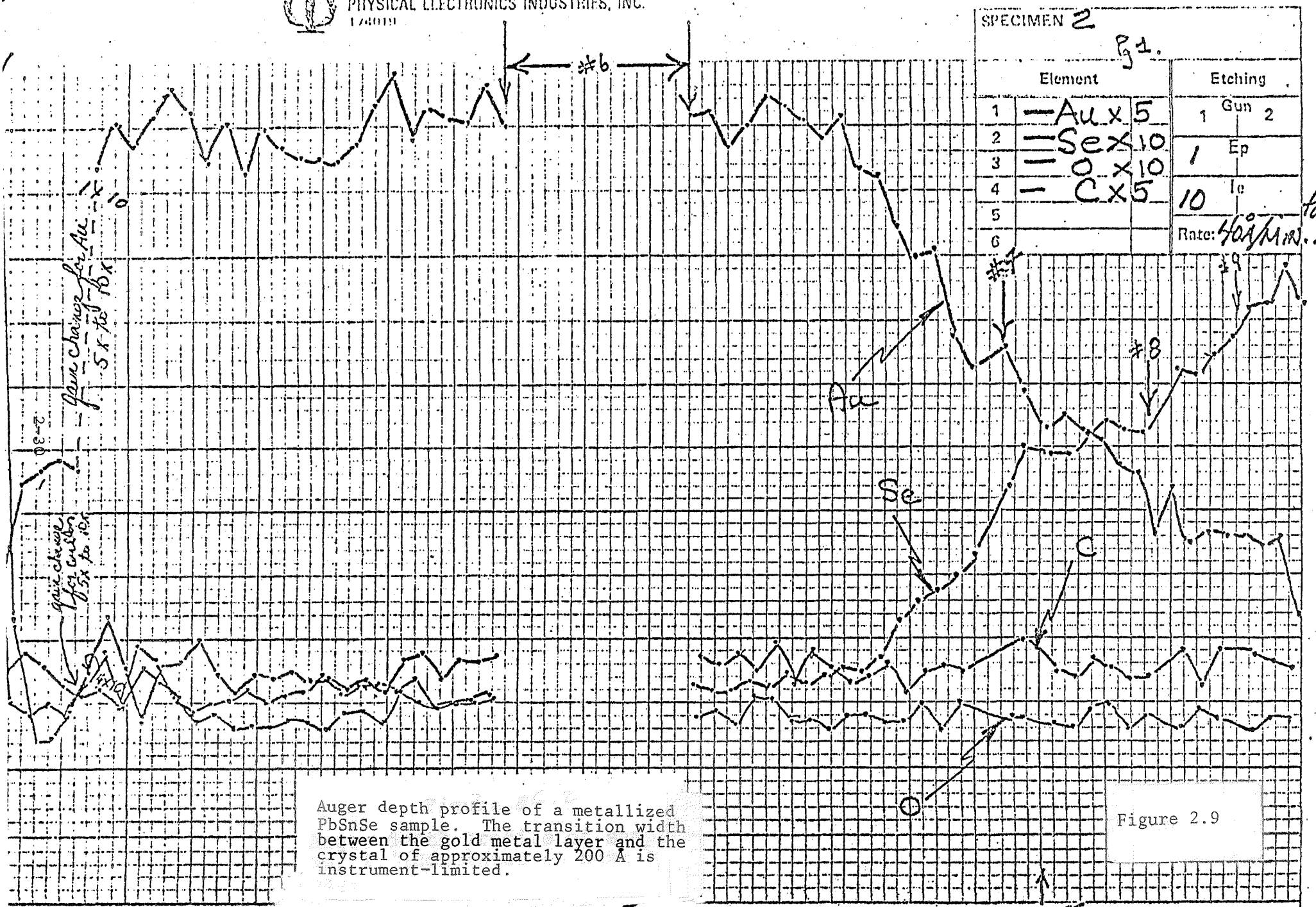

Auger depth profile of a metallized PbSnSe sample. The transition width between the gold metal layer and the crystal of approximately 200 Å is instrument-limited.

Figure 2.9

TIME, 5 MINUTES/DIVISION

Ep= 5	Ip= 5	Vmod= 3	RC=.1	Vmult.=1300	SENS= 20	NEUT. —	DATE: 8-22-78 BY: PhM

Lasers had been fabricated from portions of the wafers and lifetime data could to some extent be correlated with AES results. For these measurements, the metal layers were removed by pulling with tape and the underlying crystal surfaces examined. While no metal was visible after the layers were removed, one would expect a residue of several monolayers to remain. Methods and results are discussed in the following paragraphs.

Wafer D700:

This wafer was a p-diffused striped wafer to $Pb_{0.93}Sn_{0.07}Se$. Metallization consisted of a 2000 Å In layer on the n-side and a double layer of 2000 Å of Au followed by 2000 Å of In on the p-skin. All lasers fabricated from this material exhibited significant contact degradation within a few months.

The p-skin was examined using AES, after removal of the metal contacts. Results indicated a barely measurable amount of Au (less than 0.5 atomic % but several atomic % of In). After sputter-etching of about 150 Å of material, no In or Au was observed. Line scans across a striped region were taken with AES instrument locked to In and Au signals. Results shown in Figure 2.10, demonstrate that the residual metal is much more pronounced on the crystal than the CaF_2 insulator At the time of AES examination, the metallized material was 7 months old.

Wafer D1002:

This was an n-diffused non-striped wafer of $Pb_{0.9189}Sn_{0.011}Se$, matallized with 2000 Å of Au, 200 Å of Cr and 2000 Å of In on the p-side, and 2000 Å of In on the n-skin. Degradation was very pronounced after a few days on several lasers.

Both sides of this wafer were examined. The n-side signal indicated 5 atomic % of In and no Au. The p-side showed 2 atomic % of both Au and In. At the time of the AES study, the metallized material was 2 weeks old.

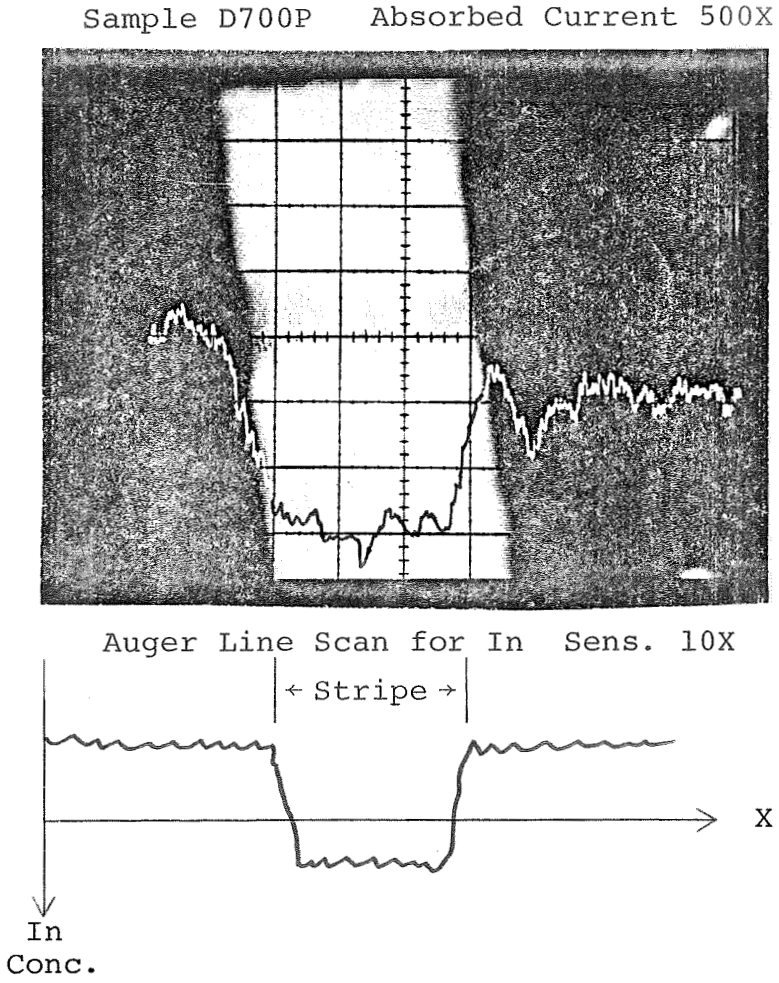

Figure 2.10

Line scan of In across striped PbSnSe sample No. D700.

Wafer D448:

This was an n-diffused, striped wafer of $Pb_{0.935}Sn_{0.065}Se$. The metallization consisted of 2000 Å, 400 Å Cr and 2000 Å In on the p-side and 2000 Å of In on the n-skin. Performance results were mixed. One laser showed no degradation after 13 months, while six other devices developed significantly higher series resistances in the same period. All lasers fabricated from this wafer a year after initial metallization had series resistances in excess of 100 milliohms and were not useable.

The p-surface was examined. Results showed the presence of about 5 atomic % of Au and no measurable In. At the time of the AES study, the metallized material was 2 months old.

Several important conclusions can be drawn from these AES experiments. The widespread presence of residual trace amounts of Br on etched crystals indicate the need for an improved post-etch rinsing and cleanup procedure. It should be noted, however, that there is no evidence that a small quantity of Br in what is probably a chemically inert compound at the metal-semiconductor interface affects performance of lifetime. The large amount of In and small amount of Au found under Au/In contacts confirms that migration of these elements does occur and that the original Au layer in contact with the crystal no longer exists after a period of time.

2.2.1.5 Investigation of Alternative Contact Metals

Results of experiments described in previous subsections clearly show that Au-In contacts do not retain their integrity and, in time, become effectively In contacts. They also show that In (on aged Au-In) contacts to both p- and n-type $Pb_{1-x}Sn_xSe$ degrade over time periods of from a few days to over a year.

The mechanism of the degradation is not known, although hypotheses can be made based upon the data and will be discussed in Section 3.1.2 of this report. However, whatever the mechanism, it is

clear that (1) if In is to be used as the bonding material, it must make electrical and thermal contact to either a p-type of n-type crystal through a different metal and (2) if Au is used to contact the crystal directly, a third metal must be sandwiched between this Au and the In to prevent interaction.

The metal used in the contacts must, of course, be reasonably easy to deposit and maintain good adhesion throughout chip processing steps such as cutting and cleaving. We have had limited success with Au/Cr/In contacts as shown by the analysis on Wafer D448 (Section 2.2.1.4). However, results for Cr as the barrier layer on production lasers have not generally been good. It is believed that, at the thicknesses required for good adhesion during processing, ($\lesssim$500 Å), the Cr layers are easily ruptured during packaging. We have also had success with a Pt barrier layer. Although this metal is somewhat difficult to deposit reproducibly by evaporation (high evaporation temperatures) or plating (possible contamination).

This sub-section describes a set of experiments in which several processing metal combinations were systematically examined for use as contacts on $Pb_{1-x}Sn_xSe$ bulk crystals. The goal was to decide upon an optimum metal combination for use with diode lasers. Bulk samples were used having the same dimensions as lasers (1/2 mm long, 1/4 mm wide and 1/4 mm high) and were mounted in standard Laser Analytics laser packages. Portions of this work were begun before the initiation of the present program and were carried into it.

In order to control the thickness of plated layers, a separate series of experiments was first carried out to calibrate plating rates. Controlled plating was found to be a somewhat difficult process, since to obtain reproducible results, it was necessary to almost continually monitor the solution pH and carefully maintain a constant temperature. With use of fresh plating solutions monitored for proper pH values it was found that reasonably consistent thicknesses resulted. Plating thickness calibrations were carried out using a Sloan Model M 100 Angstrometer. The calibration data are summarized in Table 2.7. These data indicate approximate plating rates of 800 Å/min for gold and 1000 Å/min for platimum.

Table 2.7

Electroplating Thickness Calibration Data

Obtained with an Interferometer Thickness Gauge

Material	Plating time (minutes)	Measured thickness (Å) ± 200
gold	2	1600
	4	3000
	8	6000
platinum	1	600
	2	2000
	3	3000
	5	4700

Plating details:

gold: Orotemp 24, 65°C at 1.55 volts

platinum: Technic Pt N, 95°C at 2.5 volts

Samples with the following contact metal layers (on both sides of the p-type material) were prepared (all thicknesses given in Å). Four samples for each configuration were fabricated and tested.

A. Evap 2000 Au/200 Cr/2000 In
B. Evap 1000 Au/500 Cr/2000 In
C. Evap 1000 Au/500 Ni/2000 In
D. Evap 2000 Pt/2000 In
E. Evap 500 Au/2000 Pt/2000 In
F. Plated 200 Pt/200 Au/2000 In

The first-listed metal was that in contact with the crystal. All samples were prepared from crystal G196 (7.6 % PbSnSe). These samples were tested in a liquid helium dipstick for the electrical characteristics (IV curves) at time intervals approximately 1 week apart. The results of these retests, as tracked over a 1 month period, are summarized in Table 2.8.

The evaporated Au/Cr/In and Pt/In systems are characterized by resistance increases of over an order of magnitude after 28 days, while the other 3 configurations do not exhibit any significant changes in contact resistance over this same period. All contacts were made to different portions of the same crystal (No. G196, with x = 0.076, p-type with a carrier concentration of 2.6×10^{19} cm^{-3}). The prefix E denotes evaporated metals, while the prefix P indicates plated contacts. The total observation time covered by Table 2.8 is 28 days. Since the samples from sets A, B and D deteriorated so rapidly, they were not further retested. The samples from groups C, E and F were retested at intervals 44 days, 67 days, 84 days, 100 days, and again at 152 days after fabrication. These retest data are shown in Table 2.9. It is clear that with one possible exception, none of the samples exhibit any significant increases in contact resistance over this 5 month shelf storage period (an experimental error of $\pm$ .002 Ω can be expected, since different dipsticks were used).

Table 2.8

Summary of Electrical Contact Resistance Values (ohms) Measured On

5 Different Metallization Configurations of the Same Crystal

Sample		t = 0	t = 9 days	t = 15 days	t = 28 days
E Au/Cr/In	A1	.007	.076	.238	.68 non linear
2000/200/2000	A2	Open*	2.33	.255	> 10
(Angstroms)	A3	.03*	> 1	Open	Open
	A4	.0055	.055	.0505	.275
E Au/Cr/In	B1	.2275			
1000/500/2000	B2	.047	-**	.210	.405
	B3	.18			
	B4	.0265	.25	.486	.54
E Au/Ni/In	C1	.004	.004	-**	.0035
1000/500/2000	C2	.0035	.004	-**	.004
	C3	.0035	.0035	.0035	.003
	C4	.0035	.0035	.0035	.003

*Recompressed

**Apparent dipstick problem, since resistance values of .008 ohms were obtained.

Table 2.8 (continued)

Sample		t = 0	t = 9 days	t = 15 days	t = 28 days
E Pt/In	D1	.0055	.043	.103	.208
2000/2000	D2	.0055	.032	.093	.184
	D3	.005	.013	.035	.09
	D4	.0055	.021	.0555	.128
E Au/Pt/In	E1	.003	.003	.0025	.003
500/2000/2000	E2	.0045	.004	.0038	.004
	E3	.004	.004	.004	.0035
	E4	.0045	.004	.0045	.004
P Pt/Au/In	F1	.004	.005	-**	.0045
200/200/2000	F2	.004	.005	-**	.0047
	F3	.008	-**	.008	.008
	F4	.007	-**	.005	.0045

**Note: These data were taken in a dipstick which had later been found to yield erroneously high resistance values.

Table 2.9

Update on Resistance Values Measured on p-type $Pb_{0.924}Sn_{0.076}Se$

Bulk Samples Contacted with Different Metallization Configurations

Sample	Contacts	Time after fabrication (days)								
		t=0	t=9	t=15	t=28	t=44	t=67	t=84	t=100	t=152
C1	E Au/Ni/In	.004	.004	*	.0035	.004	.004	.0038	.0038	.0042
C2	1000/500 /2000	.0035	.004	*	.004	.004	.004	.0034	.0037	.0038
C3		.0035	.0035	.0035	.003	.004	.004	.0036	.0035	.0037
C4		.0035	.0035	.0035	.003	.004	.004	.0037	.0036	.004
E1	E Au/Pt/In	.003	.003	.0025	.003	.0035	.0038	.0036	.0037	.0044
E2	500/2000/2000	.0045	.004	.0038	.004	.004	.004	.0036	.0038	.004
E3		.004	.004	.004	.0035	.004	.0044	.004	.0043	.005
E4		.0045	.004	.0045	.004	.0045	.0045	.005	.0045	.005
F1	P Pt/Au/In	.004	.005	*	.0045	.005	.005	.004	.0043	.005
F2	200/200/2000	.004	.005	*	.0047	.005	.005	.005	.0047	.0055
F3		.008	*	.008	.008	.005	.0053	.0047	.0047	.0055
F4		.007	*	.005	.0045	.009	.0095	.008	.008	.01

*Note: These data were taken in a dipstick which had later been found to yield erroneously high resistance values.

Based upon the results for p-type $Pb_{1-x}Sn_xSe$ a set of experiments was carried out on n-type material with the following contact configuration (both sides).

G. Evap 2000 Au/1000 Ni/2000 In (piece 1, linear dimensions <1 mm)
H. Evap 2000 Au/1000 Ni/2000 In (piece II, linear dimensions ≈5 mm)
I. Evap 2000 Au/1000 Pt/2000 In

The crystal composition was x = 0.024. Initial results, covering a 3 months period are summarized in Table 2.10. Note that n-type samples generally exhibit a smaller initial series resistance than p-type of the same dimensions; in fact, the RA products of about 4×10^{-7} ohm-cm^2 per side may be the lowest reported for any semiconductor device.

Stability measurements were continued for one group of 4 bulk devices from each of the p-type and n-type sample groups. Of the p-type samples, group C was tracked while of the n-type samples, group H (units 8328-1,2,3 and 4) were tracked. This retest period covered 17 months for the p-samples and 14.5 months for the n-samples. The contact resistance results obtained during this period are shown in Figure 2.11. The resistance stability of these devices is excellent, a fact attesting to the integrity of the electrical contacts as well as to the quality of the diode laser package.

Two sets of experiments were carried out to further examine plated contacts. Both n- and p-type samples were used. Metal layer thicknesses and stability results are summarized in Tables 2.11 and 2.12. The terms (ground) and (cleaved), listed in the left-hand columns of these tables, indicated the method used to thin the respective wafers. Plated In thicknesses are approximately 1 μm in every case. The stability of many of the plated contacts is excellent, although the yield of stable devides is not as good as with evaporated contacts. Because of this lower yield and the generally more difficult techniques involved, the study of plated contacts was discontinued.

Table 2.10

Summary of Resistance Values Measured on Bulk n-Devices

Metallized with Evaporated Layers.

Crystal No. G279 ($Pb_{0.976}Sn_{0.024}Se$).

GROUP	Sample	Contacts	time after fabrication (days)				
			t = 0	t = 21	t = 33	t = 50	t=90
G	8319-5	E Au/Ni/In	.0022	.0018	.010	.0015	.001
	-6	(2000/1000/2000)	.002	.0034	.0033	.003	.0025
	-7	(Small crystal	.002	.002	.0018	.0018	.0015
	-8	~ 1 mm)	.0024	.0025	.0025	.0025	.0025
H	8328-1	E Au/Ni/In	.001	t = 9 .001	t = 21 .001	t = 38 .0008	t=78 .0005
	-2	(2000/1000/2000)	.001	.0015	.0007	.0007	.0005
	-3	(Larger piece)	.001	.0013	.0008	.0008	.0005
	-4		.001	.001	.0008	.001	.0195
I	8332-1	E Au/Pt/In	.0036	t = 8 .0025	t = 20 .0025	t = 38 .0022	t=78 .002
	-2	(2000/1000/2000)	.0017	.002	.002	.0018	.0015
	-3		.0018	.002	.0025	.002	.0015
	-4		.004	.010	.0138	.010	.011

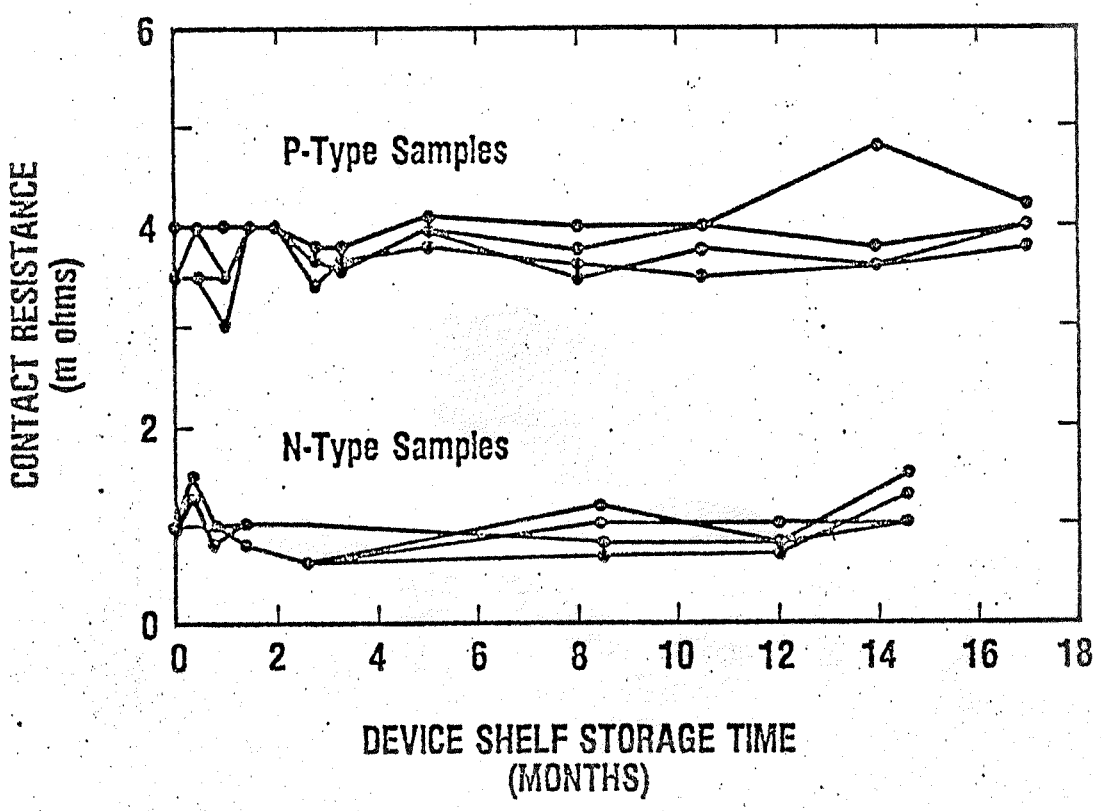

Figure 2.11

Contact Resistance Stability of n-type and p-type PbSnSe Samples Over a 15-17 Month Period.

Table 2.11

Summary of Resistance Values Measured on Bulk p-samples of PbSnSe Metallized with Electroplated Contacts. The bulk carrier concentration is 1.5×10^{19} cm^{-3}.

Sample	Contacts	Time After Fabrication (Days)					
		t=0	t=21	t=29	t=47	t=60	t=88
8326-9	2000 Au/1000 Pt/In	.0038	.004	.0043	.004	.004	.0035
8326-10	(ground)	.0032	.0032	.0032	.003	.003	.003
8326-11	Pt-Ni Plating Solution	.0030	.0030	.0031	.003	.0028	.003
8326-12		.0034	.0033	.0034	.0032	.003	.003
8326-13	2000 Au/1000 Pt/In	.0062	.0065	.007	.007	.007	.011
8326-14	(Cleaved)	.0060	.0055	.0057	.0058	.0055	.045
8326-15		.0060	.0060	.0068	.006	.0056	.006
8326-16		.0068	.0065	.0068	.0075	.0074	.0075
			t=11		t=29	t=42	t=70
8338-1	2000 Au/2000 Pt/In	.006	.0055		.0056	.0055	.006
8338-2	(Cleaved)	.007	.0066		.0067	.0067	.007
8338-3		.007	.0066		.0065	.0065	.0066
8338-4		.0075	.007		.007	.007	.0074
			t-11				
8338-25	2000 Au/2000 Pt/In	.0045	.0041		.0044	.0042	.0045
8338-26	(Ground)	.006	.0082		.0136	.018	.019
8338-27		.0047	.005		.005	.005	.0055
8338-28		.0085	.008		.008	.0075	.0085
					t=20		t=58
8362-21	2000 Au/2000 Ni/In	.0024			.0026		.0028
8362-22	(Ground)	.0029			.0029		.0033
8362-23		.0025			.0025		.003
8362-24		.0032			.0032		.0035

Table 2.12

Summary of Resistance Values Measured on Bulk n Samples of $Pb_{.968}Sn_{.032}Se$ Metallized with Electroplated Contacts

The bulk carrier concentration is 4×10^{19} cm^{-3}.

Sample	Contacts	Time After Fabrication (Days)				
		t=0	t=15	t=29	t=42	t=70
8335-13	4000 Au/2000 Pt/In	.001	.0015	.0011	.0009	.0005
-14	(Cleaved)	.0255	.031	.031	.033	.026
-15		.0055	.029	.05	.13	---
-16		.002	.0026	.0025	.0024	.0025
						t=82
8338-21	2000 Au/1000 Pt/In	.0007	.0005	.0009	.0005	.0008
-22	(Cleaved)	.0008	.0008	.001	.0005	.001
-23		.0007	.0005	.0009	.0005	.001
-24		.001	.0005	.0009	.0008	.0018
8338-29	2000 Au/2000 Pt/In	.001	.0275	.056	.17	.11
-30	(Cleaved)	.0008	.005	.014	.024	.043
-31		.0009	.0025	.0036	.0037	.0045
-32		.0009	.0016	.0014	.005	.0017

2.2.1.6 Contacts to Diode Lasers

Based upon the results of Section 2.2.1.5, several production lasers were fabricated using evaporated contacts, with 1000 Å of Au, 2000 Å of Pt, and 2000 Å of In. Operating characteristics for four lasers from three separate wafers were tracked over a 15 month shelf storage period, beginning in October, 1978. The lasers were periodically installed in dipsticks for V-I curve and relative power measurements near liquid He temperature. The laser materials were as follows:

Laser No.	Material	Expected Emission Frequency (cm^{-1})
8292-1	$Pb_{0.966}Sn_{0.034}Se$	900 cm^{-1}
8292-2	$Pb_{0.966}Sn_{0.034}Se$	900 cm^{-1}
8292-10	$Pb_{0.927}Sn_{0.073}Se$	600 cm^{-1}
8303-22	$Pb_{0.927}Sn_{0.073}Se$	600 cm^{-1}

The series resistance, threshold current and relative quantum efficiency at 2 amps were monitored, and results are presented in Figure 2.12. Series resistances for the four devices are stable to within measurement error for the four devices indicating no contact degradation. The increased threshold current for 8303-22 is outside of the limit of error and may be due to package induced strain caused by temperature cycling; there was no corresponding increase in leakage current. Apparent variations in relative quantum efficiency (which is a measured rate at which the output power increases with current near threshold) are probably due to the use of different dipsticks with different detectors for the various measurements.

The stability of the emission spectra of one of these lasers (No. 8292-2)is shown in Figure 2.13. This figure shows the 11 K emission spectrum at 2000 mA taken on October 20, 1978 and again on November 13, 1979, over one year later. On both test dates the emission spectrum is dominated by 3 strong modes. The 6 cm^{-1} shift toward higher energy may be due to an increase in thermal resistance of the contacts, indicating a slight degradation, but may also be due to differing thermal

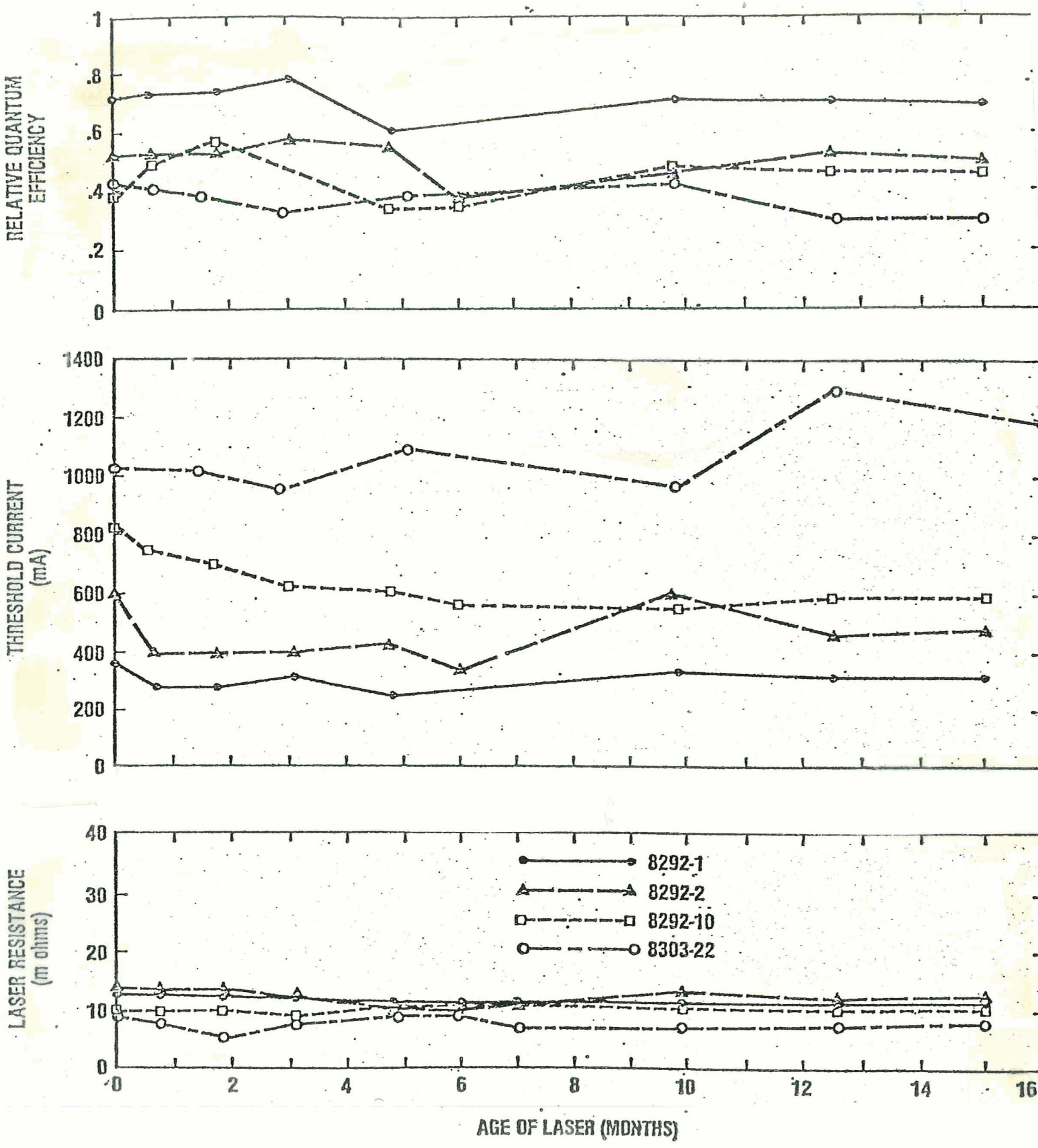

Figure 2.12

Plots of Relative Quantum Efficiency, Threshold Current and Laser Contact Resistance as Functions of Shelf Storage Time Covering a Period of Over One Year.

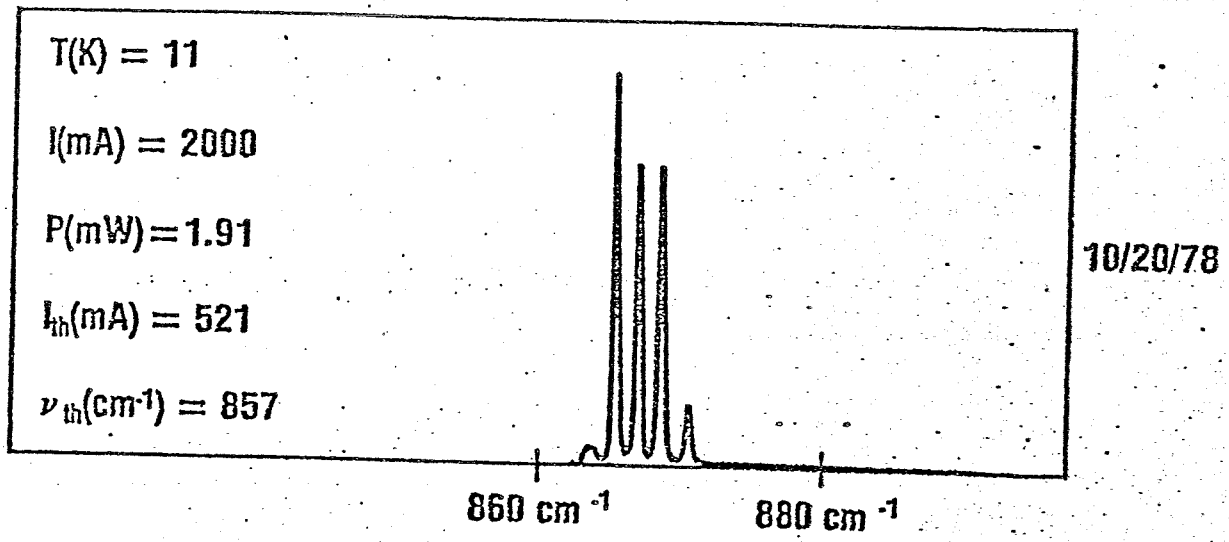

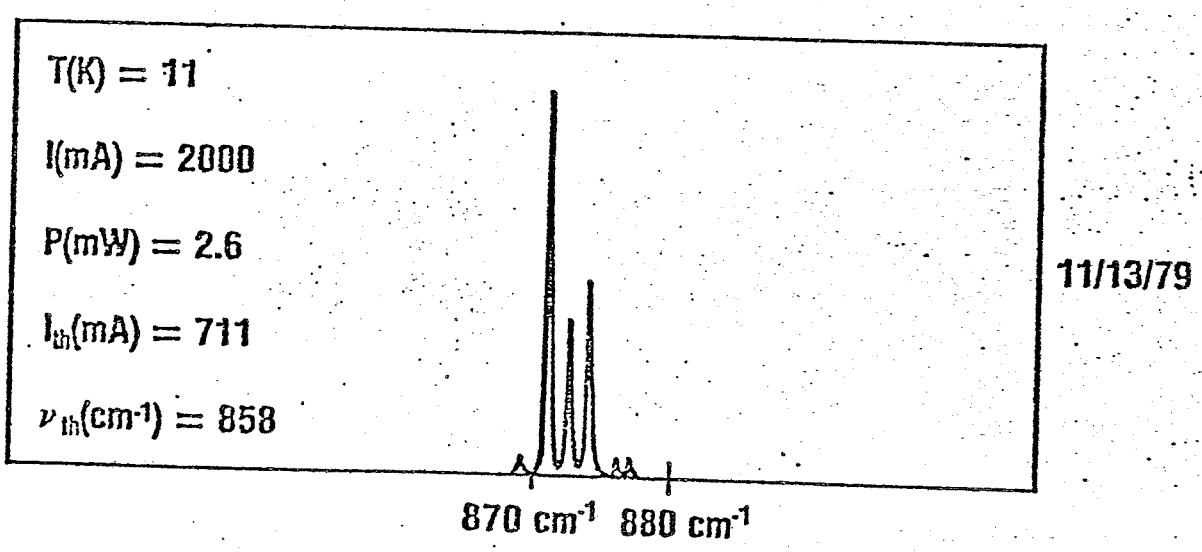

Figure 2.13

Comparison of emission spectra from laser 8292-2 taken on October 20, 1978 and again on November 13, 1979. In both cases, I = 2000 mA, CW. Differences in power reading could, in part, be due to different power meters. The shift of 6 cm^{-1} towards higher wavenumbers is possibly due to a slight thermal resistance increase.

impedances at the interface between the laser package and the dipstick mounting plates. The apparent increase in power is thought to be due to an incorrect power calibration on the first test.

Additional data on laser stability will be presented in Section 2.2.2 (where a group of lasers which were temperature cycled 500 times and then shelf-stored is discussed) and in Section 2.4 (where lasers delivered to NASA/Langley and LASL are discussed).

2.2.2 Failure Due to Temperature Cycling

One mode of failure often noted in Pb-salt diode lasers operating at cryogenic temperatures was a large increase in contact resistance caused by cycling a device between room and cryogenic temperatures. Since the lasers operate at cryogenic temperatures, this is a serious problem. Laser Analytics, Inc. believes that careful design of its heat sink package has greatly reduced the severity of this problem. An experiment was conducted to demonstrate that $Pb_{1-x}Sn_xSe$ lasers manufactured by Laser Analytics, Inc. could withstand 500 cycles between room temperature and 77 K, without significant change in its characteristics.

A station was designed and constructed for this purpose consisting of a dipstick which held 2 lasers at a time (both pointing towards a Ge:Cu photodetector which allowed for determination of threshold current and relative output power). This dipstick was automatically lowered into a large liquid nitrogen container, kept there for 10 minutes (the laser reached 80 K after 2 minutes) and then pulled out and kept in a room ambient for 20 minutes (the laser warmed to room temperature after approximately 7 minutes). This cycle was repeated every half hour, thus requiring approximately 10 days for the full 500 cycles. After the first 135 cycles the lasers were evaluated to obtain an intermediate point in the cycling schedule. During characterization, both the volt-ampere curves and threshold current (I_{th}) of each laser were measured. A total of 3 lasers were used in this test, one as an uncycled control sample and two as the cycled samples. These lasers were fabricated from wafers metallized in the same manner

as samples 8335-21, 22, 23 and 24 in Table 2.13. The results of the retests following 135 and 500 temperature cycles are shown in Table 2.13. None of the samples show any significant changes in either R_f or I_{th}, except for the control sample which appears to have had an initial I_{th} value >2000 mA, although this may have been due to a measurement error because the subsequent threshold current values appear to be relatively stable.

These lasers were subsequently shelf-stored and retested over a 1.25 year period. These retest data are summarized in Table 2.14 which tracks not only R_f and I_{th}, but also the relative quantum efficiency (ΔP) and the relative maximum output power (P_{max}) over this time period. These parameters (ΔP and P_{max}) were obtained during the electrical test evaluation of the laser by measuring the current through a copper-doped Ge photoconductive detector biased at constant voltage. This detector, located in a liquid helium dewar immediately adjacent to the diode laser, has a response current proportional to the incident photon flux. The parameter ΔP is defined as the change in log of the detector current divided by a change of 100 mA of laser current above threshold. It therefore is related to the differential quantum efficiency of the laser just above threshold. The parameter P_m is proportional to the log of the detector current at the maximum laser current (generally 2 Amps), and is therefore an approximate measure of the maximum relative output power of the laser. It can be seen that all of these lasers are relatively stable over this time period. Thus we have documented data on 2 lasers which were temperature cycled approximately 512 times (including the retest cycles) and shelf stored for over one year with virtually no changes in the laser's electrical and optical output power values. This finding represents strong evidence of a stable laser package and a major improvement in the electrical contacting.

2.3 Stripe Geometry Formation

2.3.1 General Approach

The approach for this portion of the program was (1) to form stripe geometry lasers by diffusion masking with widths much less than the standard LAI stripe of 50 μm, and (2) to fabricate stripe geometry lasers

Table 2.13

Stability Data of Lasers Cycled 500 Times Between 300 K and 77 K

Bulk crystal was p-type with an n-diffused junction depth of 16 μm.

	Original Data		After 135 temp cycles		After 500 temp cycles	
Laser No.	R_f (ohms)	I_{th} (mA)	R_f (ohms)	I_{th} (mA)	R_f (ohms)	I_{th} (mA)
8324-11	.005	1410	.006	1360	.005	1320
8324-12	.006	1270	.005	1200	.005	1200
8324-10* (control)	.005	> 2000	.005	1380	.005	1350

*Laser 8324-10 was a control sample from the same lot. This laser was not temperature cycled.

Table 2.14

Comparative Stability Data for Three Temperature Cycled

$Pb_{1-x}Sn_xSe$ Lasers Stored for Over One Year at Room Temperature

Laser	Test Date	R_f (ohms)	I_{th} (mA)	ΔP	P_{max}	Laser History*
8324-10	11-20-78	.007	>2000	--	--	Control sample -
	12-07-78	.006	1380	43	78	No special
	12-18-78	.006	1350	71	109	cycling.
	1-08-79	.006	1280	58	93	
	2-08-79	.005	1330	59	102	
	2-24-79	.006	1350	69	104	
	5-25-79	.006	1500	54	90	
	11-06-79	.006	1330	49	97	
	2-20-80	.006	1400	40	90	
8324-11	11-20-78	.005	1490	50	84	
	11-27-78	.005	1410	49	88	
	11-30-78	.006	1360	52	90	Cycled 135 times
	12-07-78	.005	1320	53	95	Cycled 365 times
	12-18-78	.006	1300	50	90	77-300K
	1-08-79	.006	1260	59	103	
	2-08-79	.005	1250	52	95	
	2-24-79	.006	1220	52	96	
	5-25-79	.005	1160	50	98	
	7-26-79	.006	1250	48	98	
	11-06-79	.006	1210	46	96	
	2-20-80	.006	1180	52	100	
8324-12	11-20-78	.006	1350	48	82	
	11-28-78	.005	1270	43	85	
	11-30-78	.006	1200	51	96	Cycled 135 times
	12-07-78	.006	1200	52	95	Cycled 365 times
	12-18-78	.005	1250	51	91	77-300K
	1-08-79	.006	1220	50	96	
	2-08-79	.006	1230	48	90	
	2-24-79	.006	1260	42	86	
	5-25-79	.006	1160	43	94	
	7-27-79	.006	1360	35	76	
	11-06-79	.006	1400	23	65	
	2-20-80	.006	1310	30	70	

*All lasers stored in air at room temperature between tests.

with several stripe widths (25, 12 and 5 μm), and (3) evaluate the lasers and analyze results to obtain an estimate for D of equation (1). These efforts will be described in the following sub-sections.

2.3.2 Electrical Contacts

The first task was to develop reproducible and reliable techniques for depositing contact metals with the new stripe dimensions and using the improved metallizing procedures discussed in Section 2.2. For this purpose insulators with the desired stripe pattern were deposited on planar-diffused, non-stripe crystal surfaces. In this configuration the entire surface of the wafer has a p-n junction, but electrical contact to this surface is made through stripes opened in an electrically insulating layer deposited on the wafer after diffusion. This processing was intended to establish all procedures except those needed to obtain diffusion stripes. Contact stripe widths of 12 μm were used. After opening the stripes in the insulator, approximately 1-3 μm of material was removed from the exposed regions by chemical etching. This premetallization etching step was found to result in improved metal adhesion. The junction depth of this wafer was determined to be 9 μm from thermoelectric probing of an angle-lapped portion. A schematic diagram of a cross-section of this wafer (D1785, with a composition of $Pb_{0.955}Sn_{0.045}Se$) is shown in the top portion of Figure 2.14, while the bottom portion is an electron beam micrograph of this wafer taken at 1240X, showing one stripe of the wafer after the etching and metallization operations. The round regions on the insulator are due to small accumulations of evaporated metal. The etched stripe region is relatively smooth although the depth of 2-3 μm presents a problem since metallization discontinuities occur at the edges of the stripe. In fact, a higher magnification revealed a slight undercutting of the crystal at the stripe edges causing the insulator to overhang by approximately 1 μm. The effects of undercutting are overcome by the subsequent indium deposition step which causes the entire surface to be covered with metal.

Lasers were fabricated from this contact-striped wafer and from an identical wafer with no contact stripes. The similar resistance values measured on lasers from both wafers indicate that the contacts to the

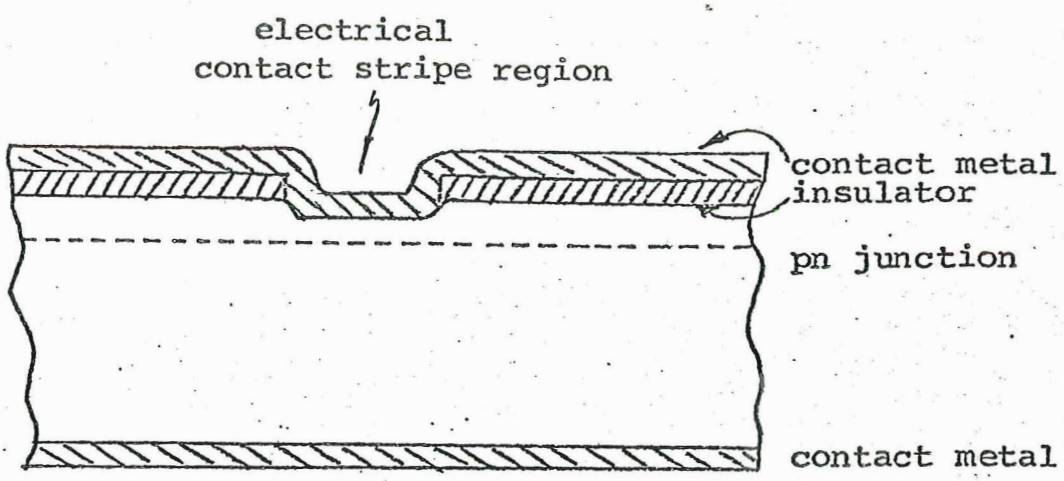

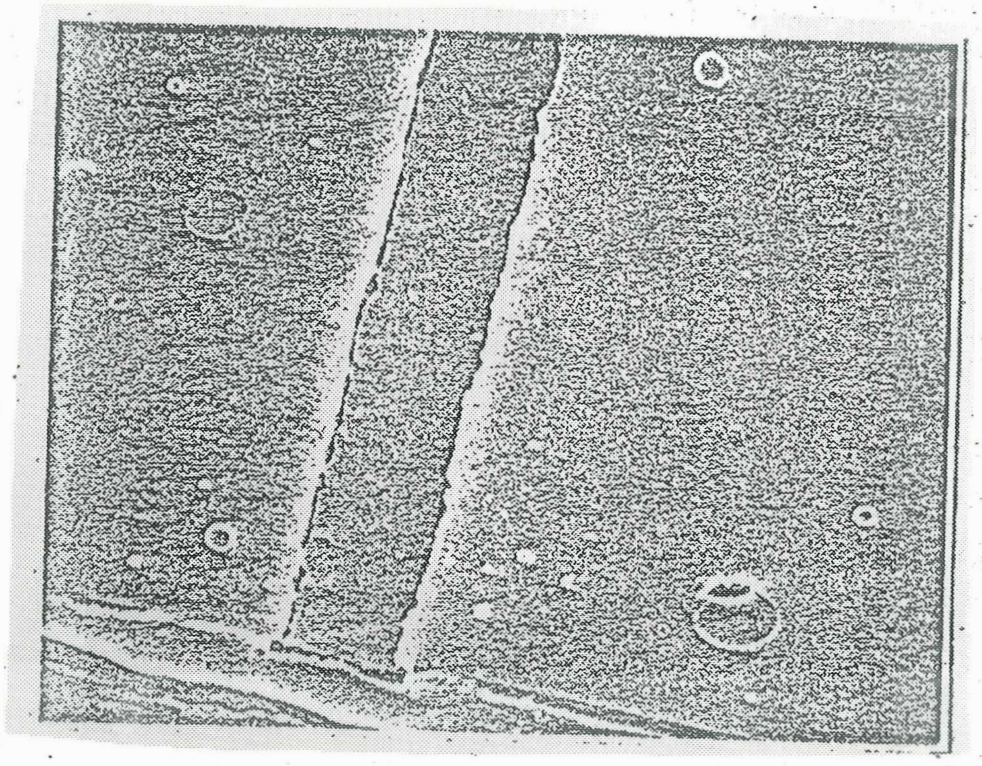

Figure 2.14

Top: Schematic Diagram of a Cross-section of Wafer D1785S Showing Electrical Contact Stripe Configuration. Bottom: Electron Beam Micrograph of This Same Wafer taken at 1240X Magnification Showing One Contact Stripe Opening in the Insulating Layer. Stripe Width is 12 Microns.

unstriped p-surface probably dominate the series resistance (as expected). A few lasers from each wafer were electrically tested and evaluated for optical output. The results are summarized in Table 2.15 and in Figure 2.15.

There is no significant difference in threshold current or emission properties between the contact striped and non-striped lasers, even though the electrical contact areas on the facet side of the laser crystal are almost 10 times smaller for the striped than for the non-striped devices. This is expected in view of the analysis of the preceding subsection and corroborates the conclusion reached there. These lasers were retested approximately 6 weeks after manufacture and exhibited no significant changes in electrical contact resistance. We conclude from these experiments that we are able to make low resistance, reliable electrical contacts to striped Pb-salt lasers with widths as narrow as 12 μm.

2.3.3 Stripe Geometry Lasers Formed by Diffusion Masking

Prior to and during the current program, internal R&D funds were utilized to develop a reliable diffusion masking technology which had been used for fabricating Pb-salt lasers with stripe widths of 50 μm. The technique for fabricating diffused-stripe diode lasers of $Pb_{1-x}Sn_xSe$ consists of the following general steps:

a. Crystal facet separation and thinning
b. Diffusion mask deposition
c. Stripe pattern definition
d. Junction diffusion
e. Diffusion mask removal
f. Insulator deposition
g. Insulator stripe definition
h. Wafer thinning and cleaning
i. Metallization
j. Cleaving to laser die size
k. Mounting of laser die into laser package

Table 2.15

Electrical and Optical Test Results Obtained from Lasers

Fabricated from a Contact-Stripe Laser Wafer

The bulk material is p-type, with an n-diffused junction depth of 9 μm.

Wafer	Laser No.	Electrical Contact Resistance (ohms)	Threshold Current (mA)	Tuning Range (cm^{-1})	Max CW Output Power (mW)	Max Operating Temp. (K)	Single Mode Tuning Range (at 15K)(cm^{-1})
1785	9318-2	.0025	600	761-884	1.40	50	0.72
(not striped)	9318-3	.015	420	759-912	2.35	45	1.10
	9318-4	.010	995	764-815	0.94	32	1.20
1785 S	9312-3	.0043	810	763-855	2.00	43	1.00
(12 μm contact	9344-15	.014	550	766-990	1.55	61	0.38
stripes)	9346-9	.019	1280	757-833	0.12	28	0.33

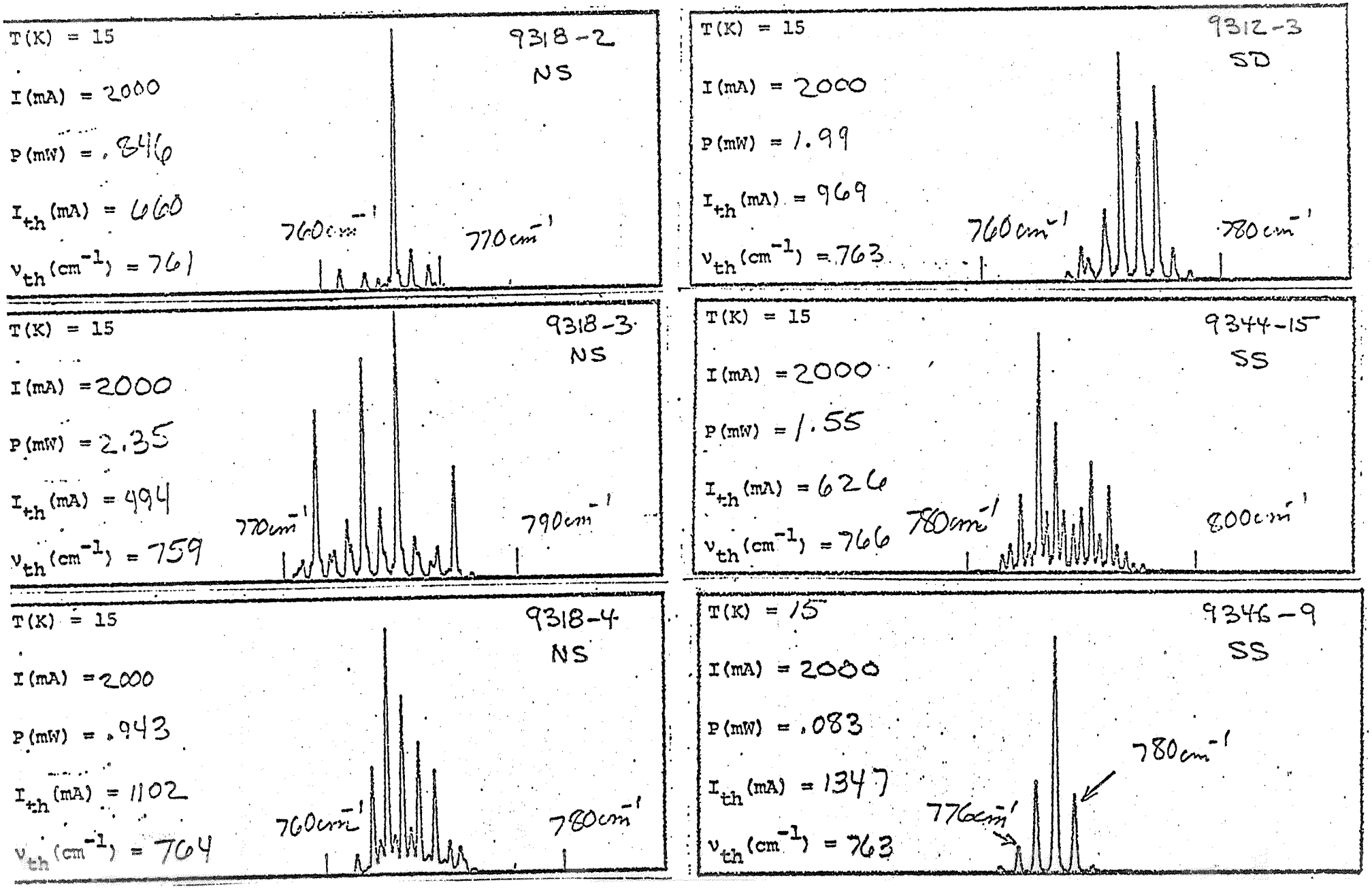

Figure 2.15

Emission Spectra of Lasers from Wafer D1785 at 2000 mA and 15 K. The 3 Lasers on the Left Side are not Striped (NS) While the 3 lasers on the Right Side are Contact Striped (SS).

Special photomasks were designed and ordered with 4 quadrants, to provide a non-striped area and 5 μm, 12 μm and 25 μm wide stripes. These widths represent the diffused region widths. The widths of the electrical contact regions were total area, 4 μm, 10 μm and 20 μm, respectively. A drawing of the mask is shown in Figure 2.16. The accuracy of the Kasper 2001 P mask aligner was adequate for achieving a 1 μm alignment reproducibility as required for the 5 μm wide stripes. To obtain this resolution, it was necessary to maintain a very close spacing between the photomask and the $Pb_{1-x}Sn_xSe$ wafer. This required the use of shims with height increments of 25 μm. Direct contact between the photomask and the wafer had to be avoided.

Etch pit density studies were carried out on several samples to determine the extent of surface damage resulting from deposition of the diffusion mask. This was done by comparing two identical pieces of the same crystal, one not coated and the other with the insulating material applied and then chemically removed. Etch pit density (EDP) measurements were then made on both crystals. Results are shown in the photographs of Figure 2.17. The left photograph shows the EPD on the wafer which has not seen the diffusion mask material. Except for a small region, there are a few etch pits on this wafer. The photograph on the right side shows the much higher EPD observed on the piece which was covered with the diffusion insulator. This same observation was made in a second identical experiment and it appears to indicate surface damage induced by the diffusion mask deposition process. The depth of this damage is also not known at present. Subsequent evaluation of lasers has not indicated that the surface damage beneath the insulator has an adverse effect on performance.

Two crystals of PbSnSe were processed into diffused-striped laser configurations. These crystals (G777 and G779) had compositions X = 0.034 and 0.032, respectively, with as-grown p-type carrier concentration of 2.5×10^{19} cm^{-3} for both. Some pertinent properties of lasers with 10 μm stripes fabricated from these two crystal wafers is given in Table 2.16. The 10 μm width stripe laser had an electrical contact resistance of approximately twice that of the 25 μm wide laser. The threshold current for the

LTR	REVISIONS	APP'D	DATE

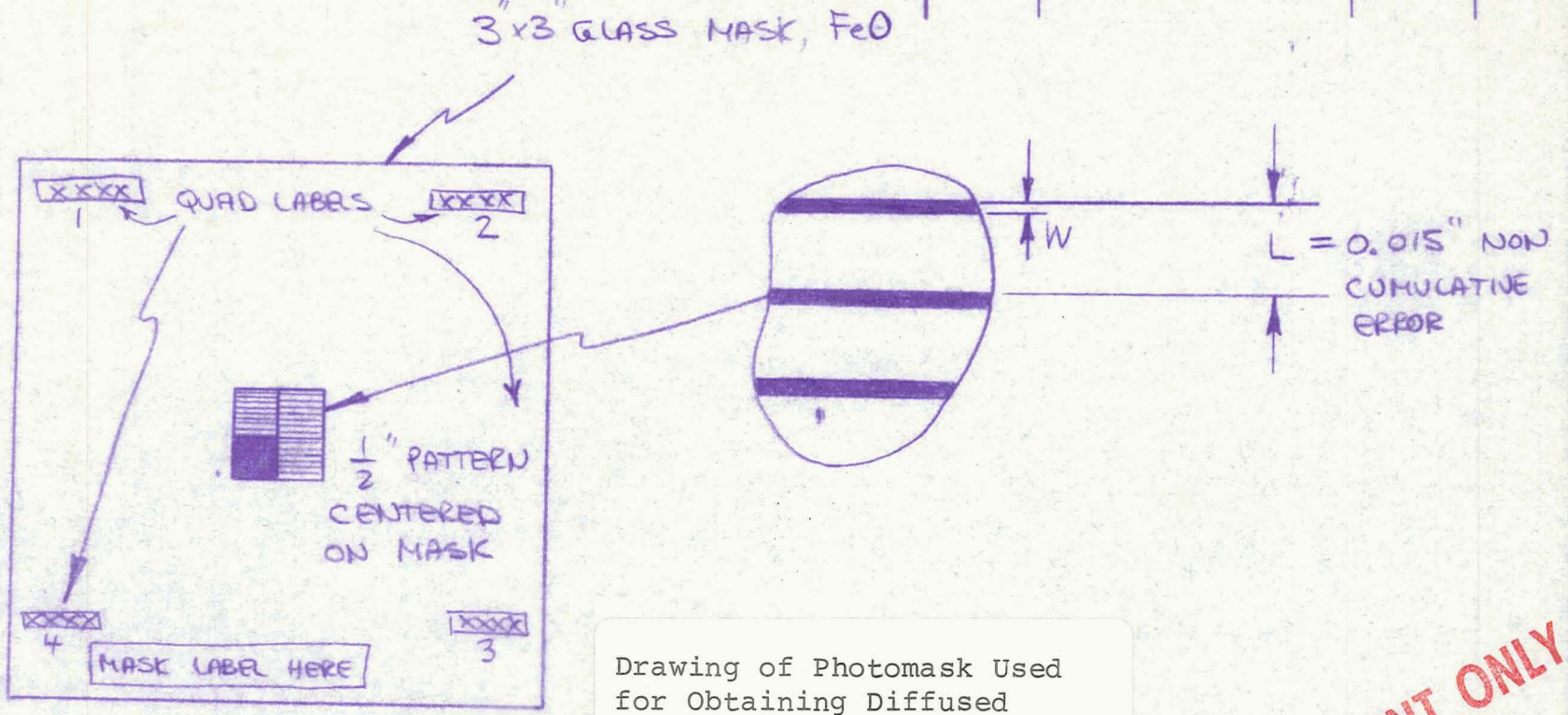

Drawing of Photomask Used for Obtaining Diffused Stripe Lasers With Various Stripe Widths.

Figure 2.16

MASK NO.	QUAD.	W	QUAD LABEL	MASK LABEL
800-054	1	.00020	5 MICRON	DIFFUSION MASK 800-054
	2	.00050	12 MICRON	
	3	.00100	25 MICRON	
	4	ALL DARK	NON-STRIPE	
800-054-1	1	.00015	4 MICRON	CONTACT MASK 800-054-1
	2	.00040	10 MICRON	
	3	.00080	20 MICRON	
	4	ALL DARK	NON-STRIPE	

LASER ANALYTICS, INC.

SCALE: NONE	APPROVED BY	DRAWN BY K. LINDER	
DATE: 12/21/79		~~TOLERANCE~~	
MAT'L: FEO GLASS MASK		± .XX	± .010
FINISH: —		± .XXX	± .005
TITLE: 5,12,25 MICROMETER STRIPE MASK		DRAWING NUMBER 800-054	

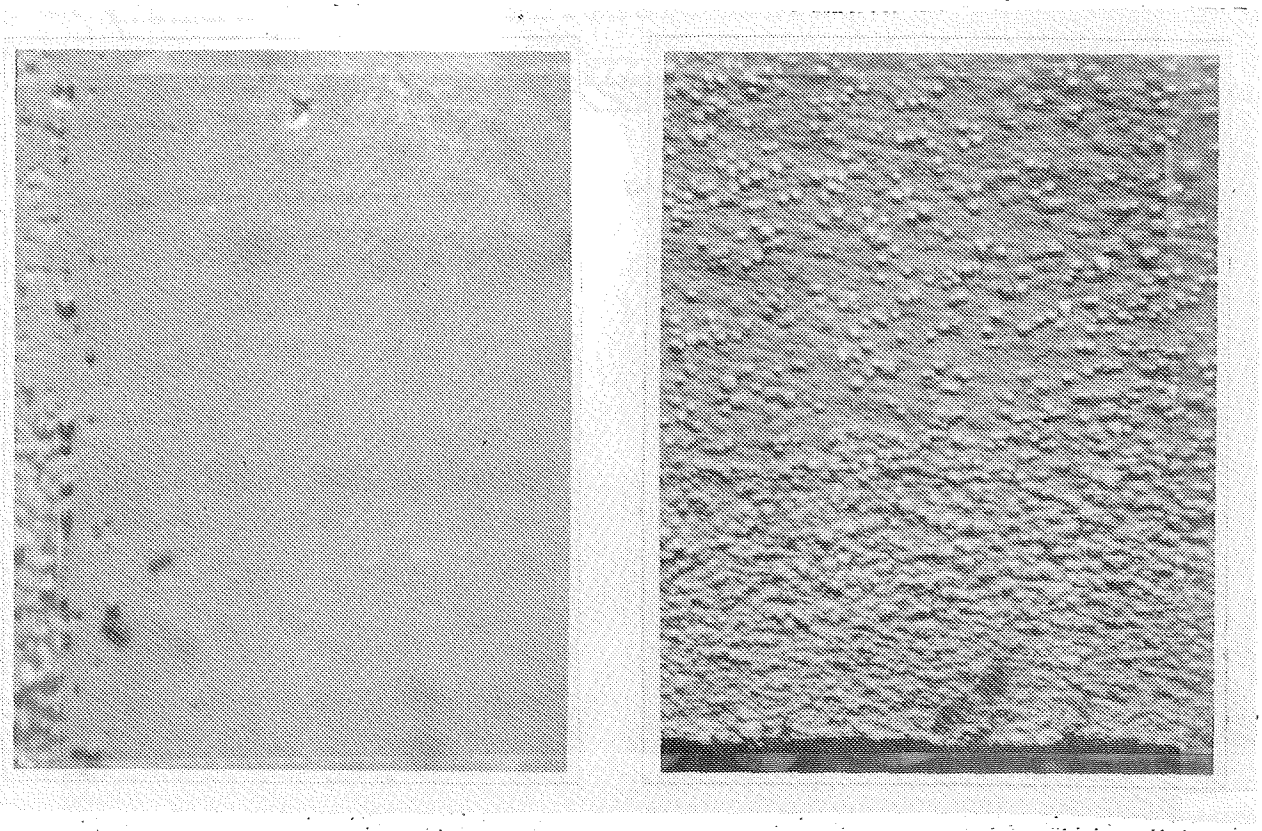

Figure 2.17

Photomicrographs of Two Sections of the Same Crystal, the Left One As-grown and the Right One Previously Coated with Diffusion Masking Materials. Both Surfaces Have Been Subjected to an EPD Measurement. Magnified 40X.

for the narrowest stripe device was the lowest of the three (310 mA) while the 25 μm stripe lasers has a 986 mA threshold current. Similar observations were made for wafer G779. The threshold currents for all devices fabricated from crystal G777 as obtained during our electrical test are shown in Table 2.17. The average values indicated at the bottom of the table indicate the trend. The shorted device of D1948 was not included in this average.

Representative emissions spectra for a non-stripe layer and a 12 μm stripe laser (both from crystal G779) are shown in Figure 2.18. for comparison. The stripe geometry device exhibits a series of well-defined longitudinal modes with little discernible evidence of satellite lines. The mode structure of the non-stripe device is less well defined and at least two strong modes exhibit satellites.

An additional set of 4 crystal wafers was processed into diffused-stripe lasers during the latter part of the contract period. In this case, each wafer was diffused prior to cutting into quadrants, but each quadrant was identified with a separate wafer number, as indicated below.

Stripe Series Ident.	Wafer No.	Crystal Number	X-Value (1%)	p-type Carrier Concentration (cm^{-3})	Stripe Width (cm^{-3})
18	2020	G832	1.5	1.2×10^{19}	Full
	2019				5
	2021				12
	2022				25
22	2082	G830	4.5	2.6×10^{19}	Full
	2083				5
	2084				12
	2085				25
24	2118	G874	2.5	1.4×10^{19}	Full
	2119				5
	2120				12
	2121				25
25	2114	G874	4.5	2.2×10^{19}	Full
	2115				5
	2116				12
	2117				25

Crystal No.	G777 (x=3.4%)			G779 (x=3.2%)	
Diffn. No.	1945	1948	1947	1949	1951
Laser No.	0025-36	0025-17	0025-13	0025-26	0023-18
Stripe width	none	25 μm	10 μm	none	10 μm
Contact resistance (ohms)	.011	.012	.027	.007	.044
I_{th} (mA) at 17K	987	330	310	730	318
T_{max} (K)	21	41	68	44	45
Spectra at 2000 mA at ~17K	some even spacing	some even spacing	some even spacing	some even spacing	mostly even spacing
Spectra at 100-130% of I_{th} at 17K	some even spacing	no even spacing	mostly even spacing	some even spacing	all even spacing at I=1.25 I_{th}
Spectra at T_{max}	2 good modes	good	fair	fair	single mode
Tuning range (17K) (cm^{-1})	not meas.	>.5	>.5	>.5	>1
Tuning rate at 17K (MHz/mA)	not meas.	206	144	144	361

Table 2.16

Performance Comparison of Stripe and Non-stripe Lasers Fabricated from Two Different $Pb_{1-x}Sn_xSe$ Wafers
All laser cavity lengths were 1/2 mm.

Table 2.17

Summary of Threshold Current Values Observed
for All Devices Fabricated from Crystal G777 (Run #12)
Laser cavity lengths were 1/2 mm.

Stripe Width	D1945 non-striped (1/4 mm width)	D1945 25 μm stripe	D1947 12 μm stripe
Measured laser threshold current values (mA)	2000 2000 2000 860	320 1180 780 1250 250 580 short ckt.	520 110 960 110 200 400 240

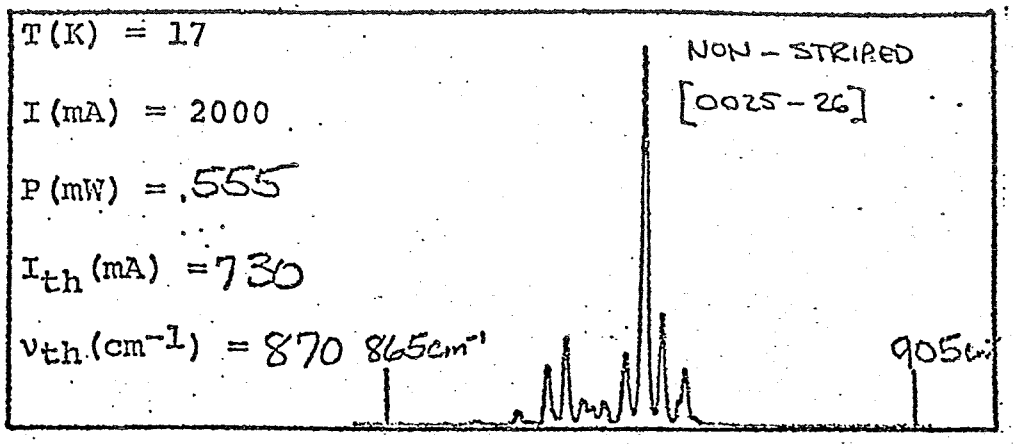

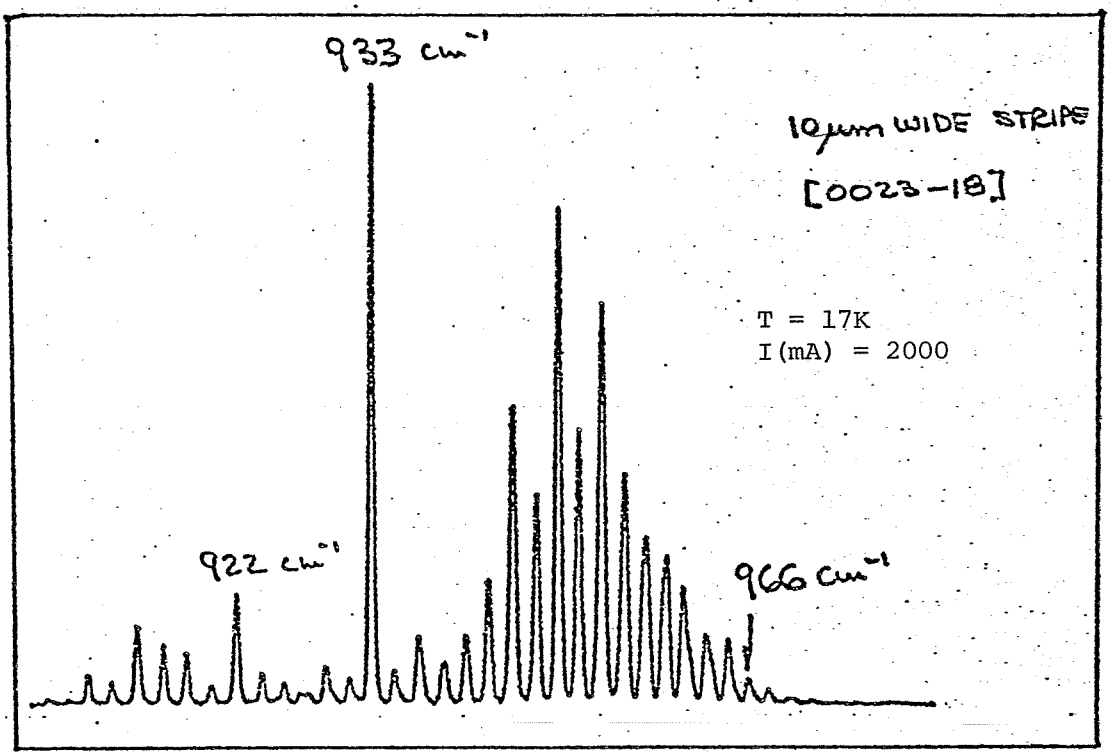

Figure 2.18

Emission Spectra of Lasers 0025-26 (Top Curve, Non-striped Laser) and 0023-18 (Bottom Curve, Striped Laser) at 2000 mA.

A summary of the results obtained from these four wafers is given in Table 2.18. Each wafer has four D-numbers assigned, corresponding to each of the four quadrants. The comments in the "process results" column indicate the observations made by the laser assembly technicians and are related to the cleaving quality of the wafers. The figures under the YLD column indicate the yield of useful laser (3/4 indicating a yield of three good lasers out of four which were assembled). The figures under the I_{th} column indicate the lowest (top) and highest (bottom) value of threshold current observed from lasers made from the particular stripe width. Junction depths, as measured by thermal probing angle--lapped portions of the wafers, are given in the bottom portion of the left hand column of Table 2.18 for each of the four series. The deep junction for G830 reflects the problems discussed in Section 2.1.3 and prevents any meaningful conclusions from being drawn for this run. The comments under "mode structure" in the optical test are self-explanatory. The following observations can be made from the data presented in Table 2.18.

a. In three of the four series, the lowest threshold occurs in one of the striped devices. Only in series #24 does the lowest threshold occur for a non-striped device. Threshold current should vary as the area, but in practice we have found it to be strongly influenced by other, materials related factors such as defect concentrations, junction depth (which can be non-uniform even on a given wafer) and cleaving quality.

b. The 5 μm and 12 μm stripe widths, when properly fabricated generally have the best mode structure. The 25 μm stripes generally exhibit more satellite mode structure.

c. The maximum CW operating temperatures occur for runs #18 (61K) and #25 (63K). Each of these runs has a relatively shallow junction (4 μm and 9 μm, repectively). The deep junction (37 μm) wafer (#22) did not yield any lasers which operated above 35 K. It is believed that

Table 2.18

Summary of Laser Results for Four Wafers Processed March - April, 1980
All laser cavity lengths are 1/2 mm.

Material	D. No.	Stripe Width (μm)	Process Results	Electrical			Optical			
				Yield	R_f	I_{th} Low / High	Tuning Range	P_m (mW)	T_m (K)	Mode Structure
PbSnSe	2020	None	Good	4/4	.02	560 / 1410	1022-1107	0.8	23	Poor definition
1.5%	2019	5	Poor Cleave	NO LASERS						
G832	2021	12	Good	3/4	.05	210 / 365				Poor electrical contacts caused overheating
#18	2022	25	Good	14/16	.03	150 / 660	1036-1096	0.2	21	Single mode
							1041-1233	1.4	61	Good modes near I_{th}
4 μm							1021-1270	0.5	45	Some spurious modes
PbSnSe	2082	None	Good	3/4	.007	420 / 1120	777-831	0.3	35	Satellite lines observed
4.5%	2083	5	Good	4/4	.01	560 / 760	770-799	0.2	23	*Poor mode structure
G830							770-842	0.3	26	Some satellite lines
#22							764-798	0.9	20	Good mode structure
	2084	12	Good	4/4	.01	375 / 1240	769-791	0.2	17	Fair mode structure
37 μm							771-848	0.2	25	Poor mode strength
							764-833	1.1	28	Many satellites
							762-823	4.5	31	*Excellent mode structure
	2085	23	Good	4/4	.02	440 / 1500	765-812	2.2	28	Fair mode structure
							767-815	0.9	21	Some satellite lines
PbSnSe	2118	None	Good	7/8	.03	150 / 1331	996-1015	0.3	25	Pronounced satellite
2.5%							943-958	0.2	17	structure
G872	2119	5	Good	2/4	.02	300 / 994	EXCESSIVE HEATING			
#24	2120	12	Good	1/4	.02	(1065)	934-1020	0.9	30	Good mode structure at 1A
4 μm	2121	25	Good	1/4	.05	(230)	926-998	0.4	27	Fair mode structure, some satellites

Table 2.18 (Continued)

PbSnSe 4.5% G874 #25 9 μm	2114	None	Good	8/8	.007	(297 652)	762-826 791	0.5 0.3	36 14	Poor mode definition
	2115	5	Good	3/4	.015	(147 628)	756-989	0.6	42	Good mode structure
	2116	12	Good	4/4	.01	(617 1635)	760-1041	1.34	63	Good structure, some satellite lines
	2117	25	Fair Cleave	4/4	.01	(183 667)	738-948	0.45	53	Pronounced satellite structure

the maximum operating temperature is determined by materials properties and junction depth and is not strongly influenced by striping.

In the case of wafer D2019 of series #18, no lasers were fabricated because of cleaving problems with this portion of the wafer. Such problems could arise from excessive grain boundaries and were complicated by the fact that this portion of the wafer was the smallest of the four sections. The excessive heating of lasers from wafer D2021 was probably caused by the relatively high contact resistance, while that of wafer D2119 probably resulted from a high thermal resistance coupled with a low operating temperature limit for all lasers made from series #24.

Attempts were made to measure the spatial profile of the emission of several stripe and non-stripe lasers. However, interference effects related to the cooler window prevented any useful data from being obtained. Development of a special cooler for this measurement was felt to be outside of the scope of this program.

The results described in this sub-section indicate that tunable diode laser performance can be significantly improved through the use of a stripe geometry configuration. From results summarized in Table 2.18 we can draw the very tentative conclusion that the maximum effective stripe width is around 12 μm. Results of spatial distribution measurements should provide more information regarding this important question. Striped lasers with 25 μm widths generally have well behaved emission spectra near threshold, but exhibited provisional satellite additional modes at higher currents.

2.4 Deliveries

2.4.1 Diode Lasers

A total of ten (10) lasers were delivered to NASA/Langley during the program period. A summary of the optical performance characteristics of these lasers is given in Table 2.19. Each of these lasers has a

Table 2.19

Laser No.	Tuning Range (cm^{-1})	Max Output Power at 15K (mW) at 2 Amps.	Power per Mode at 15K (mW) at 2 Amps
8333-16	875-1061	1.07	0.650
8333-17	862-960	0.49	0.100
9002-4	1049-1089	1.84	0.810
9002-10	1039-1097	4.21	2.700
9008-2	883-948	4.21	1.600
9008-3	874-928	1.40	0.370
9008-4	874-932	1.0	0.280
9008-8	882-950	0.77	0.265
9058-1	881-970	0.61	0.310
9058-3	881-970	0.38	0.160

List of lasers delivered to NASA/Langley during the contract period. Each of these lasers has an output power in excess of 100 μW/mode. All laser cavity lengths were approximately 1/2 mm. The electrical contact configuration for the first 2 lasers is 2000 Au/1000 Ni/thick In while that for the others is 1000 Au/1000Pt/thick In.

CW output power in excess of the 100 μW mode contractual specifications. Two of the lasers had a single mode output power of well over 1 mW. The last two lasers (9058-1 and 3) have been characterized in accordance with contractual requirements which call for current and temperature tuning rate measurements on 2 NASA lasers to be taken (a) initially; (b) after five temperature cycles to 77 K; and (c) after a 2-week room temperature storage period followed by five more temperature cycles.

The results of these cycling tests are summarized in Table 2.20. The first two rows represent both electrical and optical test data taken approximately 1 month after fabrication. The second group of two rows represent the same data taken after 5 temperature cycles between 77 and 300 K, while the third group of 2 rows represent the same data obtained after the lasers were stored for approximately two weeks and again cycled five times between 77 and 300 K. All tuning rates were obtained by use of a 1-inch Ge etalon. Since tuning rates are temperature dependent (particularly at low temperatures) the tuning rates are given for each laser at both 15K and 20K. These data are given in the fourth group of 2 rows at the bottom of Table 2.20.

A summary of the electrical characteristics of all ten NASA/Langley lasers is given in Table 2.21. This table includes all retest data carried out while the lasers were still at Laser Analytics. In some cases, this retest period was as long as 3 months. The stability of the electrical contact resistance of each of these lasers was excellent. The parameters R_f (ohms), I_{th} (mA), ΔP (arbitrary units) and P_m (also arbitrary units) indicate contact resistance, threshold current, relative quantum efficiency and relative maximum output power, respectively. Subsequent test data for these lasers obtained at NASA/LRC are given in attachments A and B.

A total of six (6) lasers were delivered to LASL during the program period. The first four lasers were delivered in March, 1979 while the other two lasers were kept at Laser Analytics for shelf storage evaluation. These two lasers were delivered to LASL on February, 1980 in accordance with the contract requirements. A summary of electrical and optical

Table 2.20

Tuning Rate Stability Measurements Made on Two of the Lasers Delivered to NASA/L During the Program. The Bottom Section of the Table Shows the Dependence of a Single Mode Tuning Rate on Laser Temperature.

Laser Number	Electrical Test				Optical Test					
	R_f (ohm)	II_{th} (mA)	ΔP (rel)	P_m (rel)	I (mA)	T (K)	Mode (cm^{-1})	$\frac{\Delta\nu}{\Delta I}$ MHz/mA	$\frac{\Delta\nu}{\Delta T}$ MHz/mK	Test Date
9058-1	.009	600	70	124	1870	20	897	48	27	3-29-79
9058-3	.009	-570	46	101	-1504	20	900	118	47	3-29-79
Lasers Cycled 5 Times Between LN_2 and Room Temperature										
9058-1	.01	600	70	125	1943	20	900	43	35	3-30-79
9058-3	NOT MEASURED				-1989	20	915	118	35	3-30-79
Lasers Stored 2 Weeks at Room Temperature and Again Cycled 5 Times from LN_2 to Room Temperature										
9058-1	.005	570	70	120	1958	20	900	45	36	4-11-79
9058-3	.005	-585	56	107	-1926	20	911	167	54	4-11-79

Note: The tuning rates $\Delta\nu/\Delta I$ and $\Delta\nu/\Delta T$ are temperature dependent, particularly in the 10 to 20K range. For the above two lasers, this temperature dependence was found to be as follows:

Laser No.	Tuning Rate $\Delta\nu/\Delta T$ (MHz/mK)	
	(T=15K)	(T=20K)
9058-1	6	36
9058-3	9	54

Table 2.21

Stability History and Electrical Characteristics of 10 Lasers

Delivered to NASA/L During the Contract Period

Laser No.		Test Date/Results				
8333-16		11/29/78	12/14/78	1/8/79	2/9/79	2/21/79
	R_f	.006	.005	.0075	.008	.008
	I_{th}	240	220	200	230	230
	ΔP	23	28	65	31	37
	P_m	93	101	119	120	100
8333-17		11/29/78	12/12/78	1/22/79	2/21/79	
	R_f	.009	.02	.025	.025	
	I_{th}	370	290	480	745	
	ΔP	65	42	33	29	
	P_m	103	78	81	75	
9002-10		1/3/79	1/22/79	2/7/79		
	R_f	.0075	.01	.0075		
	I_{th}	540	480	510		
	ΔP	72	69	72		
	P_m	121	121	124		
9008-2		1/8/79	1/22/79	2/7/79		
	R_f	.011	.011	.019		
	I_{th}	-830	-760	-1000		
	ΔP	97	85	85		
	P_m	130	130	107		
9008-3		1/8/79	1/22/79	2/7/79		
	R_f	.015	.016	.016		
	I_{th}	1050	1060	1050		
	ΔP	75	68	54		
	P_m	109	106	115		
9008-4		1/8/79	1/22/79	2/7/79	4/2/79	
	R_f	.014	.016	.015	.015	
	I_{th}	1160	1150	1330	1350	
	ΔP	76	56	57	57	
	P_m	98	97	94	91	

Table 2.21 (Continued)

9008-8		1/8/79	1/22/79	4/2/79
	R_f	.017	.019	.013
	I_{th}	1090	1020	1030
	ΔP	65	51	64
	P_m	102	97	112
9058-1		3/29/79	3/30/79	4/11/79
	R_f	.009	.01	.005
	I_{th}	600	600	570
	ΔP	70	70	70
	P_m	124	125	120
9058-3		3/29/79	4/11/79	
	R_f	.009	.005	
	I_{th}	-570	-585	
	ΔP	46	56	
	P_m	101	107	

characteristics of the first four lasers delivered to LASL is given in Table 2.22. Three of these lasers had single mode output power levels in excess of 200 μW/mode program objective and two of the lasers had multimode output power levels in excess of 1 watt at 16 μm.

As per contract requirements, two 16 μm diode lasers, fabricated in early April, 1979, were held at Laser Analytics for periodic retesting and delivered to LASL on February 22, 1980. These lasers were stored under room ambient conditions (in the normally used plastic boxes, in air at room temperature). A summary of the retest data is shown in Table 2.23. Both the electrical contact resistance and the threshold current values for these two lasers are stable to within better than 5% showing no long term trends towards degradation. The retest period covers approximately 11 months. A summary of the optical characteristics of these two lasers is given in Figures 2.19 and 2.20. Both lasers met all contract goals, exhibiting tuning ranges in excess of 50 cm^{-1} including the 627-629 cm^{-1} region at T>18 K, with a single mode power of over 200 μW. Laser 9110-3 has a multimode output power of 2 mW at 18 K.

One of the above-noted lasers, and another laser, from the same lot were evaluated for tuning rate stability during early 1979. The tuning rates were measured after several temperature cycling schedules identical to those used for the NASA lasers noted above. The results of this temperature cycling test are summarized in Table 2.24. While some differences in single mode tuning rate are evident, they are believed to be due to extraneous factors, such as small differences in the thermal impedance of the interface between the laser package and cooler mounting platform from one run to another.

2.4.2 Dipsticks

Liquid helium dipsticks, intended for use in evaluating the electrical characteristics of diode lasers, two at a time, were delivered as follows: two to LASL and one to NASA/Langley.

Table 2.22

Summary of the Electrical and Optical Test Data Obtained for Four Lasers

Delivered to LASL in March, 1979

Laser No.	Wafer Run No.	R_f (ohms)	I_{th} (mA)	ΔP (rel.)	P_m (rel.)	Tuning Range (cm^{-1})	I_{th} (mA)	Maximum * Multimode Power		Maximum Power/ Mode in the 627-629 cm^{-1} Region	
								(mW)	At T(K)	(mW)	at T (K)
9045-6	D1238B	.01	+150	80	117	588-717	+183	.699	15	.200	25
9059-18	D1237	.009	-590	73	113	558-769	-582	1.39	15	.327	28
9059-19	D1237	.009	-430	63	94	556-688	-465	.183	15	.150	25
9061-16	D1237	.005	+360	66	106	559-718	+405	1.05	34	.200	35

* All currents are near 2 amps.

Table 2.23

Stability Evaluation Data for Two LASL Lasers

Held at Laser Analytics for 11 Months Prior to Delivery

Laser No.	Test Date	Electrical Contact Resistance (ohms)	Threshold Current (mA)
9039-21	4-4-79	0.007	+330
	4-9-79	0.008	+310
	4-23-79	0.008	+320
	7-13-79	0.007	+315
	1-11-80	0.004	+300
	2-12-80	0.005	+305
9110-3	4-20-79	0.007	-430
	7-30-79	0.007	-395
	8-31-79	0.006	-400
	2-12-80	0.005	-430

TUNABLE DIODE LASER PERFORMANCE TEST REPORT

ACCOUNT NO. 5309 DATE SHIPPED 2-13-80

CUSTOMER LOS ALAMOS SCI. LAB. FINAL CERTIFICATION BY K. J. Linde

SPECIFICATIONS OF ORDERED LASER

MODEL SDL- X (CONTRACT NAS1-15190)

FREQUENCY RANGE (SPECIFIED PORTION) 627 to 629 cm^{-1}

ADDITIONAL REQUIREMENTS 50 cm^{-1} TUNING RANGE, TO INCLUDE 627-629 REGION AT T > 18K ; P > 200μW/M

PERFORMANCE OF LASER SDL- X SERIAL NUMBER 9093-21

POLARITY POSITIVE

MAX. ALLOWED CURRENT +2000 mA

MAX. OPERATING TEMP. 40 °K

OPERATING CONDITIONS TO ACHIEVE FREQUENCY RANGE:

$\nu(cm^{-1})$ = 600 at I = +2000 mA and T= 25 °K

$\nu(cm^{-1})$ = 628 at I = +2000 mA and T= 35 °K

POWER (MULTIMODE) MEASURED WITHIN FREQUENCY RANGE:

P = 0.7 mW at I = +2000 mA and T= 35 °K

THRESHOLD CONDITIONS:

$\nu(cm^{-1})$ = 547 at I = +413 mA and T= 15 °K

REPRESENTATIVE SPECTRUM

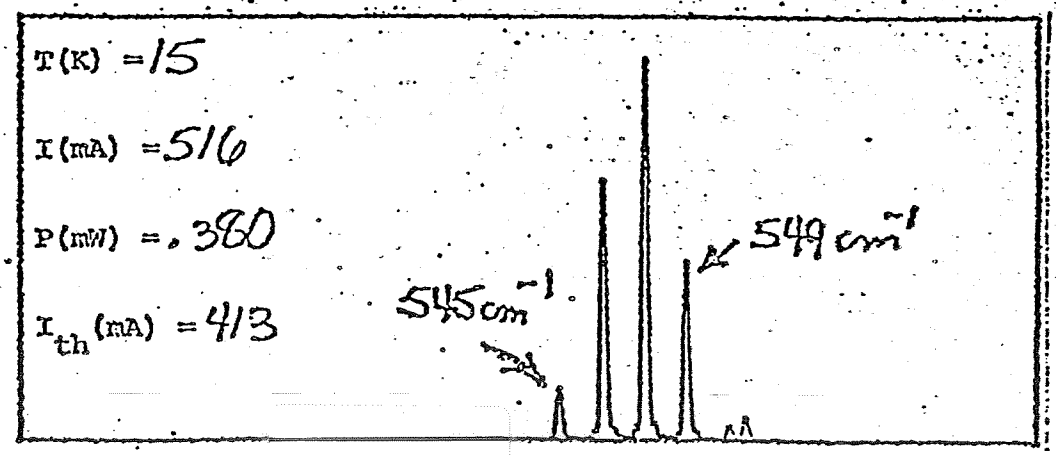

Figure 2.19

Optical characteristics of laser 9093-21, comprising one of the 2 lasers kept at Laser Analytics for 11 months prior to delivery to LASL. During this period, the laser was periodically checked for stability.

TUNABLE DIODE LASER PERFORMANCE TEST REPORT

ACCOUNT NO. 5309. DATE SHIPPED 2-13-80

CUSTOMER LOS ALAMOS SCI. LAB. FINAL CERTIFICATION BY K. J. Linden

SPECIFICATIONS OF ORDERED LASER

MODEL SDL- X (CONTRACT NAS1-15190)

FREQUENCY RANGE (SPECIFIED PORTION) 627 to 629 cm^{-1}

ADDITIONAL REQUIREMENTS 50 cm^{-1} TUNING RANGE, TO INCLUDE 627-629 REGION AT T > 18K; P > 200 μW/MODE

PERFORMANCE OF LASER SDL- X SERIAL NUMBER 9110-3

POLARITY NEGATIVE

MAX. ALLOWED CURRENT -2000 mA

MAX. OPERATING TEMP. 40 °K

OPERATING CONDITIONS TO ACHIEVE FREQUENCY RANGE:

$\nu(cm^{-1})$ = _____ at I = _____ mA and T= _____ °K

$\nu(cm^{-1})$ = 628 at I = -1160 mA and T= 19 °K

POWER (MULTIMODE) MEASURED WITHIN FREQUENCY RANGE:

P = 2.0 mW at I = -2000 mA and T= 18 °K

THRESHOLD CONDITIONS:

$\nu(cm^{-1})$ = 623 at I = -500 mA and T= 18 °K

REPRESENTATIVE SPECTRUM

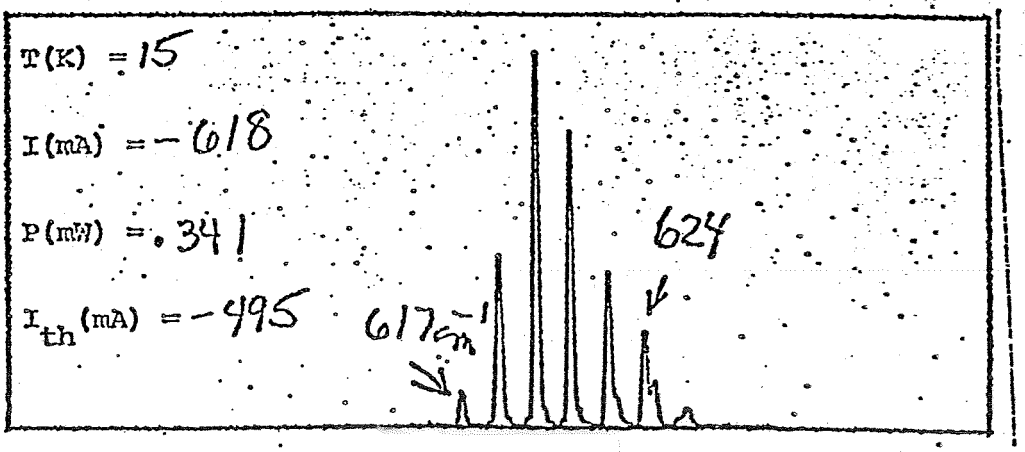

Figure 2.20

Optical characteristics of laser 9110-3, comprising one of the 2 lasers kept at Laser Analytics for 11 months prior to delivery to LASL. During this period, the laser was periodically checked for stability.

Table 2.24

Tuning Rate Measurement

Laser No.	Electrical Test				Optical Test					
	R_f (ohm)	I_{th} (mA)	ΔP (rel.)	P_m (rel.)	I (mA)	T (K)	Mode (cm^{-1})	$\frac{\Delta\nu}{\Delta I}$ MHz/mA	$\frac{\Delta\nu}{\Delta T}$ MHz/mK	Test Date
9093-21	.008	330	550	118	2000	15	551	104	10	4-5-79
9099-5	.008	-400	60	109	1780	20	628	165	30	4-9-79

Lasers Cycled 5 Times Between LN_2 and Room Temperature

9093-21	.009	310	62	122	1996	15	555	37	5	4-9-79
9099-5	.008	-400	62	109	1768	20	628	173	35	4-10-79

Laser Stored 2 Weeks at Room Temperature and Again

Cycled 5 Times from LN_2 to Room Temperature

9093-21	.008	320	90	140	2000	15	554	50	8	4-24-79
9099-5	.009	-410	68	110	1800	20	628	150	25	4-24-79

3.0 CONCLUSION

3.1 Summary and Discussion of Results

3.1.1 Materials Preparation and Characterization

A significant effort was invested in growing, processing and characterizing crystals of specific wavelength regions for the program. This included the fabrication and test of preliminary, evaluation lasers. Several observations and results from this portion of the program are believed to be of importance to Pb-salt laser technology. It was found, for example, that regions of crystal surface defects and imperfections could be identified by microscopic visual examination and EPD characterization, and that higher quality devices resulted from avoiding these regions. It was noted that a "crust" region of high defect density less than one μm thick often exists on as-grown and diffused crystal facets; such a region would be quite detrimental to device performance if it included the p-n junction.

In studying p-n junctions it was found that, with all materials parameters under rigid control, junction depths varied from less than 1 μm to over 30 μm for n into p diffusions. However, with p into n diffusion, consistent, reproducible results were obtained and a useful relation was derived. The problem may be related to formation of a surface diffusion barrier, possible an oxide layer, but we did not further pursue it. Since n into p diffusions are preferred for $Pb_{1-x}Sn_xSe$ diode lasers, further attention to the problem is needed.

3.1.2 Degradation Phenomena

It was found that shelf storage degradation is a room temperature phenomenon that can be prevented by storing lasers in liquid nitrogen. Analysis of historical data revealed that the severity of degration does not depend upon any materials related parameters such as composition, growth temperature, diffusion temperature or whether the starting crystal is

n- or p-type. It also showed that low voltage leakage currents resulted from surface effects and were unrelated to contact degradation (leakage current affects laser threshold current). Later tests showed that carrier concentrations of Pb-salt crystals do not vary measurably with time after crystal growth, hence such a variation is not involved in contact degradation.

The observation that In contacts on n-type $Pb_{1-x}Sn_xSe$ degrade severely at room temperature was unexpected and is felt to be of considerable importance. It appears as if a solid-state interaction between In and $Pb_{1-x}Sn_xSe$ similar to that known to occur between In and Au is responsible. We do not have an explanation for the effect at this time, but believe it is significant that this phase diagram of In plus Sn (a constituent of $Pb_{1-x}Sn_xSe$) exhibits a low temperature eutectic similar to that in the In-Au system.(15) Whatever the mechanism, this observation shows that it is imperative not to bond directly to either n- or p-type $Pb_{1-x}Sn_xSe$ with In.

AES studies showed that Au-In contacts do not retain their integrity and allow In to come into contact with the crystal. They demonstrate the need for a barrier metal between the Au and In. These studies also indicated that traces of chemicals used in processing steps may be difficult to completely remove.

It was found that both evaporated and plated layers of Pt and Ni provided effective barriers between Au and In films. The evaporation technique was chosen as the cleanest and most controllable. Au-Pt-In and Au-Ni-In contacts on both n- and p-type bulk crystals were found to be stable for periods much longer than a year. Lasers for delivery to NASA/LRC and LASL were fabricated using the new techniques and have remained stable for more than a year.

The integrity of the Laser Analytics laser package was found to be excellent after 500 cycles between room and liquid nitrogen temperatures.

3.1.3 Stripe Geometry Optimization

Techniques were developed to reduce stripe widths to as low as 10% of the value used in Laser Analytics' commercial devices. Preliminary tests on lasers with electrical stripe contacts on planar junctions demonstrated that, (1) reliable, sufficiently narrow contacts using the improved metallization techniques could be deposited and, (2) as expected from theory, current spreading is too pronounced to achieve an effective stripe geometry in $Pb_{1-x}Sn_xSe$ by this approach.

Processing methods were developed to achieve diffused stripe geometry lasers with widths as small as 5 μm. Surface crystal damage induced by the diffusion barrier was observed but did not adversely affect laser performance. From analysis of the spectral mode structure it was tentatively concluded that the maximum stripe width which will cut off modes of higher order than TE_0 is between 12 and 25 μm.

3.1.4 Delivered Lasers

Ten diode lasers for the 9-12 μm range meeting or exceeding contractual specifications in all respects were delivered to NASA/LRC. Four of these lasers met or exceeded the program objective of 500 microwatts per mode, the maximum being 2,700 microwatts per mode. One laser met both the 500 microwatt per mode and T > 30K objectives.

Six diode lasers for the 16 μm region meeting or exceeding contractual specifications in all respects were delivered to LASL. Five of these lasers met or exceeded the program objective of 200 microwatts per mode, the maximum being 380 microwatts per mode.

All lasers delivered under this contract met or exceeded contractual specifications with respect to operating temperatures. In addition, seven of the ten lasers delivered to NASA and all six lasers to LASL exceeded the program objectives of 30 K. The highest operating temperature for a delivered laser was 65 K.

Two LASL lasers retained at LAI for one year for shelf life studies exhibited no significant change in characteristics after more than 10,000 hours of storage at room temperature.

3.2 Recommendations for Future Work

3.2.1 Near Term

Results of the present program point to two near-term efforts that, if successful, we believe will make it possible to provide lasers satisfying the long-term objectives of 500 microwatts per mode reliably and reproducibly and at operating temperatures above 45 K. These efforts are:

(1) Obtain reliable control of junction depth. Our results showed that this critical parameter varies widely, probably as a result of surface effects. We believe that a program to develop pre-diffusion bulk and surface processing procedures will have immediate, positive results. An examination of $Pb_{1-x}Sn_xSe$ laser data recently carried out in our laboratory has shown that there is an optimum depth for maximum performance.

(2) Improve the stripe geometry preparation method. A narrow, mesa-etched stripe in a homojunction laser should give better performance than a diffused stripe because of the large refractive index step between the crystal and vacuum. However, as can be seen from Equation (1) of Section 2.3.1, a longer refractive step will necessitate a narrower stripe to suppress higher order modes. Thus the effort will require optimizing various factors.

3.2.2 Longer Term

It is apparent from results obtained over the years with III-V compound lasers that very large improvements can be expected from developing double heterostructure lasers in the Pb-salts. Preliminary research efforts at several laboratories have confirmed this idea. Recently, for example, the feasibility of lattice-matched heterojunction structures (16) and burried heterostructures (17) in $Pb_{1-x}Sn_xTe$ was demonstrated by a group at M.I.T. However, the published performance of heterojunction Pb-salt lasers has not been significantly better than that of the best homojunction laser, (1) and the present heterojunction technology is far below the stage of commercial viability. Problems in Pb-salt homojunction and heterojunction technology are believed to involve many interrelated factors, such as electrical contacts, thermal impedance, junction depth optimization, stoichiometry control, interdiffusion mechanisms, substrate crystal quality, doping levels and materials purity.

In view of 1) the importance of high quality infrared diode lasers to existing and future NASA programs and 2) the difficulties in the current Pb-salt heterojunction technology, we believe a comprehensive three-year materials and device technology effort should be embarked upon, with the long range goal of establishing a manufacturing capability for heterojunction lasers. Such an effort would include the development of a heterojunction technology, and the investigation and optimization of a wide range of materials control, fabrication and structural parameters. Based upon results obtained with the present best quality homojunction lasers, we anticipate lasers with substantially improved performance will become routinely available at the conclusion of the program; for example, we believe lasers in the 9-12 μm range with CW power outputs greater than 10 milliwatts are realistically attainable.

4.0 REFERENCES

1. K. J. Linden, K. W. Nill and J. F. Butler, IEEE J. Quantum Elect. QE-13, 720 (1977).

2. A. R. Calawa, T. C. Harman, M. Finn and P. Youtz, Trans. Met. Soc. AIME 242 , 374 (1968).

3. J. F. Butler, et al., Appl. Phys. Lett. 5, 75 (1964).

4. K. W. Nill, et al., Appl. Phys. Lett. 16, 375 (1970).

5. V. Simic and Z. Marinkovic, Thin Sol. Films, 41, 57 (1977).

6. R. G. Plumb, et al., Sol. State and Elec. Dev., 3, 206 (1979).

7. W. Lo, Japan Laser Conf., Tokyo (Sept., 1978).

8. J. F. Butler, Meeting of the IRIS Specialty Group on Infrared Standards, San Diego, (January 28-29, 1974).

9. H. Kressel and J. F. Butler, "Semiconductor Lasers and Heterojunction LED's", Academic Press, New York, 1977, Chapter 5.

10. W. P. Dumke, Sol. State Elec. 16, 1279 (1973).

11. T. C. Harman and I. Melngailis, "Appl. Sol. State Sciences", Volume 4, R. Wolfe, ed., Academic Press, New York, 1979, Chapter 1.

12. R. S. Allgaeir and W. W. Scanlon, Phys. Rev. 111, 1029 (1958). (We assume the mobility of $Pb_{1-x}Sn_xSe$ is comparable to or higher than that of PbSe.)

13. T. C. Harman and J. P. McVittie, J. Elect. Mat's., 3, 843 (1974).

14. L. J. Van der Pauw, Philips Res. Rep. 13, 1 (1958).

15. C. J. Smithells, "Metals Reference Book", Vol. II, Plenum Press, N.Y., 1967, p. 511.

16. D. Kasemset and C. G. Fonstad, IEEE International Electron Devices Meeting, Washington, DC (Dec., 1979).

17. D. Kasemset, S. Rotter and C. G. Fonstad, 38th Device Research Conference, Cornell University, June 23-25 (1980.

Attachment A

TABLE I. Summary of LaRC Test Data on Contract Lasers

	SPECIFICATION					
LASER #	#1	#2	#3	#4	#5	#6
8333-16	Yes	No	Yes	Yes	Yes	Yes
8333-17	No	No	No	No	No data available	No data available
9002-4	No	No	No	No	No data available	No data available
9002-10	No	No	No	Yes	Yes	Yes
9008-2	No	No	No	Yes	Yes	Yes
9008-3	No	No	No	Yes	Yes	Yes
9008-4	No	No	No	No	Yes	Yes
9008-8	No	No	No	Yes	Yes	Yes
9058-1	No	No	No	No	No data available	No data available
9058-3	No	No	No	No	Yes	Yes

SPECIFICATION

#1 500 μw/mode @ T $\geq$ 30K within a spectral range from 893-943 cm^{-1} or 1031-1081 cm^{-1}.

#2 500 μw/mode @ T $\geq$ 30K and at one of NASA's predetermined wavelengths (i.e., 9.20 μm or 11.20 μm).

#3 500 μw/mode @ T $\geq$ 30K with no restrictions on λ.

#4 500 μw/mode with no restrictions on T or λ.

#5 Spectral output within the spectral region 893-943 cm^{-1} or 1031-1081 cm^{-1} with no restrictions on power, temperature.

#6 A spectral mode at one of NASA's predetermined wavelengths with no restrictions on power, temperature.

1. Report No.	2. Government Accession No.	3. Recipient's Catalog No.
NASA CR-165682		

4. Title and Subtitle	5. Report Date
Development of Lead Salt Semiconductor Lasers for the 9-17 Micron Spectral Region	March 31, 1981
	6. Performing Organization Code

7. Author(s)	8. Performing Organization Report No.
K. J. Linden, J. F. Butler, K. W. Nill and R. E. Reeder	
	10. Work Unit No.

9. Performing Organization Name and Address	11. Contract or Grant No.
Laser Analytics, Inc. 25 Wiggins Ave. Bedford, MA 01730	NAS1-15190
	13. Type of Report and Period Covered

12. Sponsoring Agency Name and Address	13. Type of Report and Period Covered
National Aeronautics and Space Administration Langley Research Center Hampton, VA 23665	Contractor Report 12/22/77-4/22/79 and 11/1/79-8/15/80
	14. Sponsoring Agency Code

15. Supplementary Notes

16. Abstract

Improved diode lasers of $Pb_{1-x}Sn_xSe$ operating in the 9-17 μm spectral region have been developed. The performance characteristics of the best lasers exceeded the contract goals of 500 μW/mode at T>30K in the 9-12 μm region and 200 μW/mode at T>18K in the 16-17 μm region. Increased reliability and device yields resulted from processing improvements which evolved from a series of diagnostic studies. By means of Auger electron spectroscopy, laser shelf storage degradation was shown to be characterized by the presence of In metal on the semiconductor crystal surfaces. Studies of various metal barrier layers between the crystals and the In metal led to the development of an improved metallurgical contacting technology which has resulted in devices with performance stability values exceeding the contract goal of a one-year shelf life. Lasers cycled over 500 times between 300K and 77K were also shown to be stable. Studies on improved methods of fabricating striped geometry lasers indicated that good spectral mode characteristics resulted from lasers with stripe widths of 12 and 25 μm.

17. Key Words (Suggested by Author(s))	18. Distribution Statement
	Unclassified - Unlimited

19. Security Classif. (of this report)	20. Security Classif. (of this page)	21. No. of Pages	22. Price*
Unclassified	Unclassified	96	